MULTIPLE-RESONATOR WIRELESS POWER TRANSMISSION SYSTEM DESIGN AND INTEGRATED DATA PATH

by

Hao Wang

B.S. in Engineering, Tsinghua University, China, 2009

M.S. in Engineering, University of Pittsburgh, US, 2011

Submitted to the Graduate Faculty of

The Swanson School of Engineering in partial fulfillment

of the requirements for the degree of

Doctor of Philosophy

University of Pittsburgh

2016

UNIVERSITY OF PITTSBURGH

SWANSON SCHOOL OF ENGINEERING

This dissertation was presented

by

Hao Wang

It was defended on

November 3, 2015

and approved by

Mingui Sun, Ph.D., Professor, Departments of Neurological Surgery, Bioengineering and Electrical and Computer Engineering

Ching-Chung Li, Ph.D., Professor, Departments of Electrical and Computer Engineering and Computer Engineering

Ervin Sejdić, Ph.D., Assistant Professor, Department of Electrical and Computer Engineering

Robert J. Sclabassi, Ph.D., Professor Emeritus, Computational Diagnostics Inc.

Yiran Chen, Ph.D., Associate Professor, Department of Electrical and Computer Engineering

Zhi-Hong Mao, Ph.D., Associate Professor, Departments of Electrical and Computer Engineering and Bioengineering

Dissertation Director: Mingui Sun, Ph.D., Professor, Departments of Neurological Surgery, Bioengineering and Electrical and Computer Engineering

MULTIPLE-RESONATOR WIRELESS POWER TRANSMISSION SYSTEM DESIGN AND INTEGRATED DATA PATH

Hao Wang, PhD

University of Pittsburgh, 2016

With the rapid development of mobile and implantable devices, the wireless power transfer (WPT) technology has become increasingly attractive because it frees numerous electronic systems from power cords or batteries. Recently, the WPT method based on the magnetic resonant coupling has gained popularity both in research and applications. This dissertation contributes to the magnetic resonant WPT system design by addressing three important problems.

The first problem deals with the design of multiple-resonator systems. In order to power objects over a longer distance, a multiple-resonator system is usually needed. However, most existing multiple-resonator systems are designed experimentally with a strict requirement on the position of the resonators. We propose to optimize multiple-resonator systems by investigating the transfer function from the transmitter to the receiver. An equivalent circuit model is developed to maximize the power output. This method is then utilized to find the optimal position for the relay resonator in a three-resonator wireless power transfer system.

The second problem is to power a device which is mobile within a certain field. The Biot-Savart law and a concentric model of a spiral coil are utilized to simulate the magnetic field distribution of a multiple-transmitter WPT platform. The vertical component of the magnetic

field of the coil is optimized to achieve an evenly distributed magnetic field over the field. As a result, a position-free powering of mobile sensors or devices is achieved.

The third problem deals with integration of wireless power transfer and wireless data communication. This problem is especially importation in implanted medical sensors where power must be delivered to the implants and measured data must be transmitted to the outside of the human body. Currently, most implementations of power and communication systems utilize a separated data channel, which requires not only substantial power consumption but also a high complexity of the implanted circuit. In this work, a unified data and power channel is developed in which data are processed by an asynchronous sigma-delta pulse conversion. The resulting pulses are transmitted using load modulation.

Keywords: Resonant, Coupling, Wireless, Multiple-resonator, Transfer function, Asynchronous Sigma Delta Modulation, Load Modulation, Data Transmission.

TABLE OF CONTENTS

LIST OF TABLES

LIST OF FIGURES

1.0 INTRODUCTION

1.1 BACKGROUND

Wireless power transmission (WPT) has been a hot topic in the recent years in both academic and industrial world for the sake of releasing human from charging cords and achieving the ultimate mobility. This technology is also helpful for charging implanted devices, because the operation to change batteries of implanted devices is both inconvenient and dangerous. Even though wireless charging has coming into people's life only in the recent years, wireless power transmission cannot be considered as a new idea, but emerged over a hundred years ago.

1.1.1 The origin

In 1831, the physicist Michael Faraday introduced to the world his law of induction, which opened the door to both wireless communication and wireless power transmission. The law described how a time varying magnetic field can generate voltage in an electric circuit, and the experimental platform that Faraday used to testify this phenomena can be considered as a prototype of iron core transformer, which is an easy-to-be-ignored form of wireless power transmission because of its extremely short transmission range and the lack of mobility due to the iron core. Due to the limitations of radio frequency and power electronics technologies, people hadn't succeeded in applying this discovery to long distance transmission until the late

1800's, when two engineers, Guglielmo Marconi and Nikola Tesla, separately achieved long distance wireless communication. And Nikola Tesla moved a step further to the area of long distance power transmission.

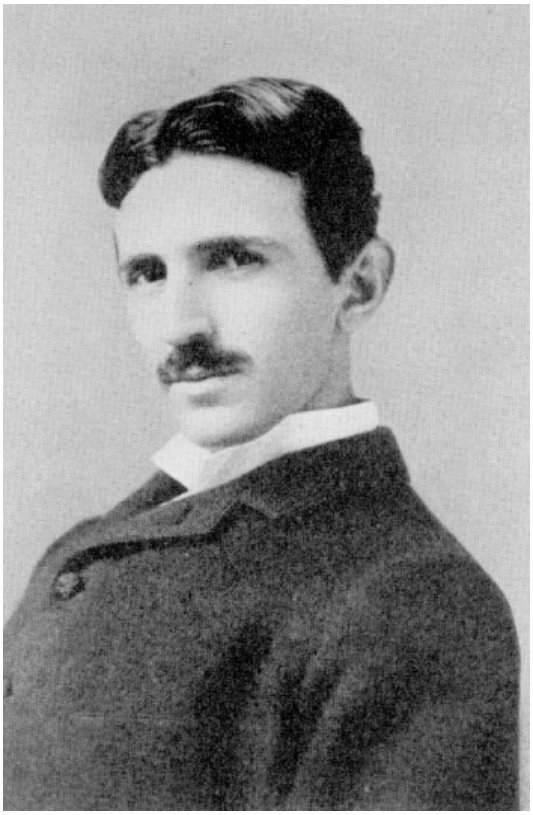

Figure 1. Nikola Tesla photo by Sarony of New York

Seventy years after his death, Nicola Tesla is still remembered as the greatest inventor in the 20th century or even the greatest in the human history because of his life-changing inventions, for example, AC motor, Tesla coil and radio. However, one of his most brilliant projects failed to come into people's everyday use and gradually faded out people's view together with the once famous Wardenclyffe Tower in Long Island. In this project, Tesla successfully lighted 200 50-watt incandescent bulbs located 26 miles away from his power transmitter, which is still applaudable even with today's technology [1]. He also got his patent "apparatus for transmitting

electrical energy" in 1914 [2]. Despite this brilliant achievement, Tesla's wireless energy transmission project was unfortunately halted because of the lack of funding. And with the great success of his another invention, the AC power grid, the research of wireless energy transmission was considered unnecessary at that time and was discarded for decades.

Figure 2. Wardenclyffe tower

1.1.2 The reviving

While mobility is becoming more and more important in people's life, the call for releasing human from the last leash, the charging cord, becomes louder. And there emerged two kinds of wireless power transmission (WPT) schemes, as known as the radiative method and magnetic induction method. Although Faraday's law is the principle behind both methods, these two methods are quite different in terms of frequency of electromagnetic wave and the transmission distance.

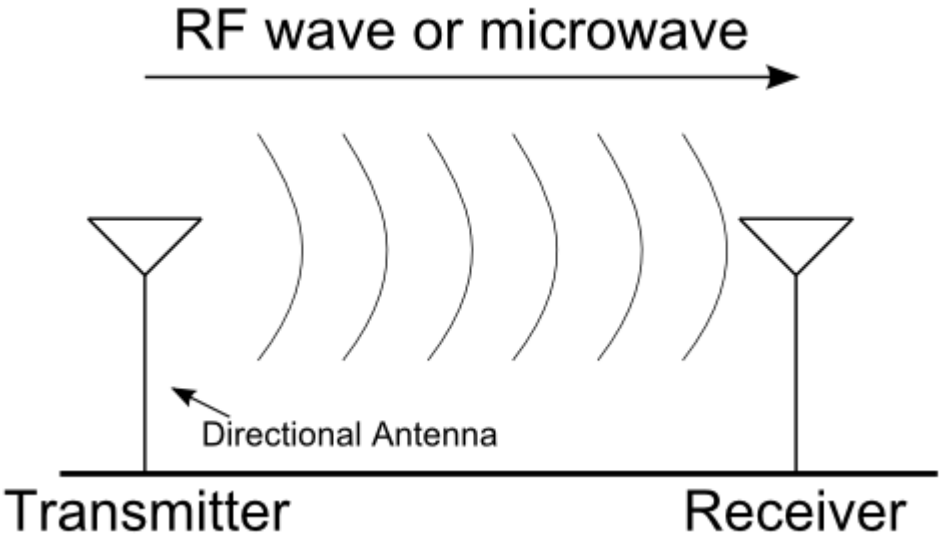

Figure 3. Sketch of radiative WPT system

The radiative method, also known as far field method, was inspired by the telecommunication technology. As we all know, people have been transmitting signal wirelessly since late 19th century using RF or microwave as carrier, which can be considered as a form of energy as well. So, in the radiative method, people use a transmission system that is quite similar to a telecommunication system, where electromagnetic wave is transmitted between the source and device antennas. The advantage of this method is that the transmission distance can be quite large, actually much larger than the dimension of the antennas. So some large scale systems were development based on the radiative scheme, among which one of the best known is the space satellite power system (SSPS) [3]. The SSPS research was triggered by a 1960's paper talking about transmitting solar energy harvested in the space. This is probably the largest man-made wireless power transmission system. Despite the long transmission distance, the radiative method, however, suffers from some major problems. In the communication field, people use omnidirectional antenna, which is far from optimal for energy transmission, as the power density

decreases following the inverse square law, and except for the small portion of energy that is intercepted by the receiving antenna, most of the energy is radiated to the space and wasted. Nowadays, with the development of antenna technology, this problem can be solved using highly directional antenna. Using this kind of directional antenna, NASA achieved 82.5% efficiency at one-mile distance in 1975 [5], and people can even achieve higher than 90% efficiency now. In this case, how to develop a highly directional antenna becomes a critical problem that people have been trying to solve and made much progress [6]. However, this highly directional antenna causes another two problems. Although the directional electromagnetic beam can be transmitted to a specific location, it is also easily blocked due to the short wavelength. So, a clear straight path is always required for this system [7]. Another problems is that when the receiver is moving, it can easily miss the beam. So, to power a moving object, a tracking system is needed, which will make the whole WPT system both more complex and more costly. A final problem of the radiative method is that the working frequency is high, in the radio frequency or microwave band, which interferes with human body strongly and is not suitable for everyday use.

Figure 4. SSPS system [4]

The magnetic induction method, on the other hand, is for short distance transmission (typically in centimeter range if not smaller) and thus it is also known as near field method [8, 9]. This method is originated in the transformer technology. The whole magnetic induction WPT system consists of two coils, namely transmitting and receiving coils. These two coils are strongly coupled to each other so that an air core transformer is formed. Thus the alternating current in the transmitter could induce voltage in the receiving coil and energy is transmitted as a result. This technology is more popular in our daily life compared to the radiative method, and to

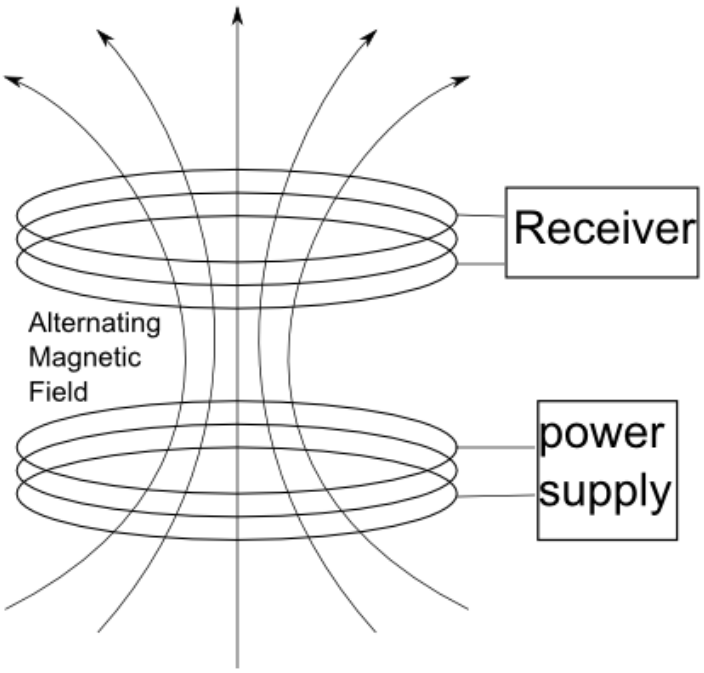

Figure 5. Sketch of a magnetic induction WPT system

name some applications, there are wirelessly charged tooth brushes and cell phones, among which the most famous one is the Qi standard developed by Wireless Power Consortium. Normally, the frequency band of this method is much lower, e.g. in the hundred kHz or lower MHz band, thus the wavelength of the electromagnetic wave is quite large (hundreds of meters)

and cannot be easily blocked. Also, as the transmitting distance is much smaller than the dimension of the coils, evanescent wave is used and no directional antenna is needed. The magnetic induction method could get high efficiency (>90%) in near field range, but the efficiency decreases quickly as the distance between the transmitting coil and receiving coil increases. Even though we successfully get rid of the iron core as in the transformer case, this method can hardly be considered as a mobile charging method due to the extremely short transmission distance.

1.1.3 The new climax

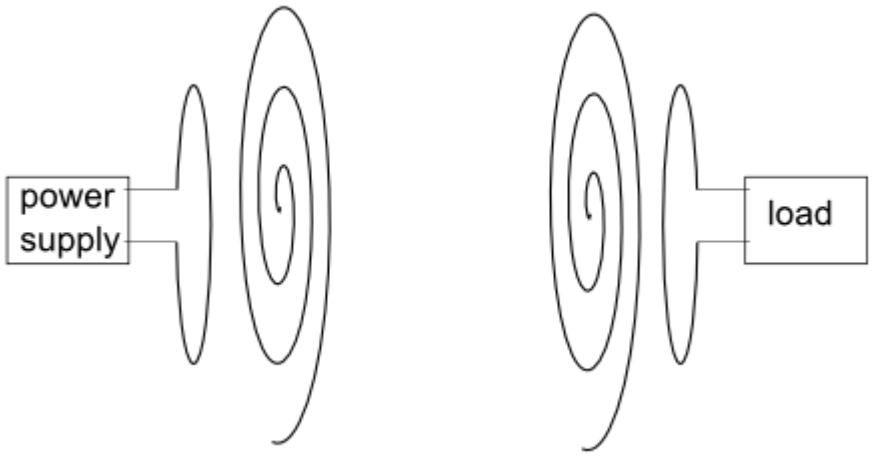

Figure 6. Sketch of two-resonator witricity system

The shortcomings of the radiative and inductive technologies greatly limited their usefulness in applications. And in 2007, an innovative WPT system, known as magnetic resonant coupling method, witricity or mid-field method, was developed in MIT, with promising performances [6, 10]. The setup of this new system is similar to that of the magnetic induction method, however instead of just two coils, two resonators are used just as in radiative method. The introducing of

resonant coupling increases the power transfer range from short range to mid-range, which can be as large as several times of the dimension of the resonators, and the increase of power transfer range in turn increases the number of applications that can apply this technology. The magnetic resonant method has no tracking or blocking problem as for radiative method and can get high efficiency at a much larger distance than the magnetic induction method could. This new technology triggered a new climax in the research of wireless power transmission, because of its promising future applications, e.g. charging electrical automobiles.

1.2 MOTIVATION

Despite the increase of transmission distance, a simple two-resonator system still cannot power a distant object or objects moving in a large area. To solve, this problem, we could use repeaters or relays to increase the transmission distance or use multiple transmitters to cover larger area. So, many researches have been focusing on the multiple-resonant systems or the so called position free system. Many research topics can be found in this area, e.g. adaptive impedance matching, frequency tracking and so on, most of which are common problems in all RF and microwave circuits. However there is a unique problem in the multiple resonator WPT system, which has not been well analyzed, that is to decide how to arrange all the transmitters and repeaters so that the receiver can get sufficient power supply in a longer distance or larger area. Despite all those works in the multiple resonator WPT area, most of those works are mostly based on experiment and there lack a systematic analysis and design procedure for a general multiple-resonator system. The reason for this is that the traditional analytical methods become too complicated to

solve when the number of resonators becomes larger (≥3). Also, the relationship between positions of resonators and the electrical behavior of the system has not been clearly understood. In this dissertation, the author tried to analyze and design a system based on mutual inductance analysis using Neumann's Formula and by optimizing either the transfer function or the evenness of magnetic field based on the applications.

Another challenge is the unification of wireless power transmission and wireless data transmission, which is essential in the current applications as most mobile and implanted devices communicate with other devices either for control commands or to transmit measured signals and other information. The mainstream approaches to combine power and data transmission is to include a separate data channel in the devices using Bluetooth and ZigBee, etc. However, a separated data channel will not only make the system more sophisticated but also increase the power consumption. These shortcomings of a separated data channel are vital for the case of implanted and mobile devices, where the size of these devices are quite limited. So a unified power and data channel is desired. However, using the power channel to transmit data also subjects to problems because of the relatively low carrier frequency and high quality factor characteristics of the WPT system. So, besides building a unified data and power transmission system, this dissertation also tries to exploit the channel capacity through a model referenced edge recovery mechanism hoping to increase the data rate.

1.3 DISSERTATION OUTLINE

This dissertation is divided into two parts, focusing on power and data transmission respectively. Chapter 2 is an overall review for both power and data transmission, including recent works on

multiple- resonator resonant coupling WPT systems and data integrated WPT system as well as some essential parts for power and data transmission, e.g. coupled mode theory (CMT), equivalent circuit model (EQM), asynchronous sigma-delta modulation (ASDM) and load modulation. The latter chapters are separated into three projects. Chapter 3 focuses on transfer function based multiple resonator WPT system design, where a three-resonator WPT system was optimized with respect to the position of the relay resonator, such that the transfer function or equivalently the power transferred from the transmitter to the receiver is maximized. In chapter 4, a multiple-transmitter platform was optimized such that the vertical component of the magnetic field generated by the platform are evenly distributed within the required range. To achieve this goal, the magnetic field was approximated by utilizing Biot-Savart law and concentric model of the spiral coil, and the evenness of the magnetic field was maximized through metaheuristic models such that a global optima can be achieved. Chapter 5 is for unified data and power transmission system. Theoretical analysis was first provided with the main focus on the model referenced edge recovery mechanism, which is also the most import contribution of this part. The experimental verification was also provided in in this chapter, where a system is built to transmit a pre-measured ECG signal. And chapter 6 concludes the whole dissertation and some discussions are included as well.

2.0 LITERATURE REVIEW

2.1 RELATED WORKS ON MULTI-RESONATOR WPT SYSTEMS

Many researches have been done on the magnetic resonant coupling WPT system since 2007, most of which use two methods to analyze this system, namely the coupled mode theory (CMT), which has been a handy tool to analyze resonators since 1950's, and the equivalent circuit method (EQC). Karalis et al developed the two-resonator witricity system based on the CMT method, the optimal coupling coefficient and load were found in terms of resonator system to get maximum efficiency [9, 10]. In 2009, Benjamin, James and Seth studied the WPT system to power multiple small receiving resonators [11]. This research is based on the circuit theory, and the small receiving resonators are placed far from each other so the coupling between the receiving resonators can be ignored. The voltage gain from source to load is evaluated and test. Andre et al also published a paper about powering multiple devices in 2010 [12]. CMT theory was used in this research, however because of the complexity of matrix inversion, the number of devices is restricted to 2, and to further simplify this model, the receiving resonators are much smaller than the transmitting resonator and are placed on different sides of the transmitting resonator symmetrically, so that the coupling of the two receiving resonators can be ignored. The result shows that the total efficiency of the three-resonator system is higher than that of a two-resonator system. In 2010, Jin-Wook et al studied the power deliver to multiple devices also

based on the CMT theory [13]. In their research, the receiving resonators were placed in such a form that the adjacent resonators were perpendicular to each other so that the coupling of receiving resonators can be ignored. The ratio between energy stored in receiving resonators and energy stored in the whole system was tested and simulated; the result shows that this ratio increases when we increase the number of devices. Alanson, David and Joshua presented their work on mid-range power transfer system using the circuit theory in 2009 [14]. In this paper, S parameters were introduced to the analysis of the system and were simulated with respect to different coupling coefficients and driving frequencies, also the idea of frequency tuning was introduced in this paper to make sure that the system is driven at optimal frequency. In the same year, Yong-Hae et al expanded the ideal of frequency tuning to multiple-receiver systems and improved the performance of multiple-resonator WPT system [15]. Not only frequency tuning, impedance matching was also considered to improve the efficiency of witricity systems [16]. Fei et al raised the relay problem about the WPT system in 2010 [17]. The response of each resonator was calculated using CMT theory and experiments were performed to find the optimal relay position so that the maximum efficiency can be achieved. Result shows that the relayed system can get much higher efficiency than the original system and the optimal relay position is around the midpoint between the transmitting the receiving resonators. Other than the CMT and EQC methods, many researches have also been done using other approaches. In 2011, Marco and Mauro attacked the system using network theory [18]. Hiroshi et al investigated the calculation of system parameters from electrodynamics and the effect of system parameters to system performance [19]. Power loss factors were evaluated numerically by Satoshi et al [20]. Hyeon-Chang et al studied the resonator design problem to maximize the efficiency [21]. Takehiro et al brought in the problem of maximizing transmission distances [22]. K. E. Koh et al studied the

impedance matching and power division problem in a multi-receiver and repeater wireless power transfer system using the technology they call impedance inverter, which could handle a chain of same resonators, with assumption that only neighboring resonators will couple with each other. Based on the simulation, they conclude that both impedance matching and the power division could be achieved using impedance inverter [23]. Hyunkeun Lim et al reported a positioning-free magnetically resonant wireless power transmission board in 2012, which is a board with staggered repeater coil array. Their experimental result shows a minimum efficiency of 64% anywhere over the board, however no theoretical analysis is provided [24].

Because CMT and EQC are the most commonly used tools to analyze a magnetic resonant coupling WPT system, they will be introduced in more detail in later sections.

2.2 RELATED WORKS ON INTEGRATED DATA TRANSMISSION

Integrating data transmission function is a natural expansion of a wireless power transmission system, as in many applications data and power needs to be transmitted at the same time, e.g. implanted physiological sensors. Even before witricity was presented, Kartikeya et al published a series of papers about a joint power and data transmission system for distributed neurotransmitter sensing, where both power and data were transferred through a pair of inductively coupled coils. The transmitted data were digital, and thus clock signal and data encoding were both needed in the implanted device [25-27]. In their 2009 paper, an EEG measurement system is capable of transmitting data at 32kb/s with a carrier frequency of 4Mz, and the working distance between transmitter and receiver can reach up to 3.5 cm. In 2013, Tolstosheeva et al developed a wireless and fully-implantable ECoG system with both power and data transmission functions [28].

However, power and data were transmitted through separated channels, where power was fed to the implants via inductive coupling, while data were transmitted through an RF transceiver. The advantage of this approach is that data can be transmitted in both direction compared to the previous approach where signal can only be transmitted from the sensor to the reader. However, a separated data channel requires the implant to generate a clock by itself and the clock frequency is much higher than the previous unified data and power channel approach. Another approach was developed by Riccardo et al in 2011 to implement a robotic capsule endoscope system, where 300mW of power can be wirelessly transferred to the capsule via inductive link [29]. The system have two separate data channel, where commands are transmitted to the capsule by directly modulate the power carrier, and the captured images were delivered to the base station through RF link. In 2011, a Japanese group tested the performance of transmitting digital data through a magnetic resonant power transmission system [30]. Their work shows that the resonant system is only capable of transmitting data at low data rate, due to the narrow bandwidth. And the bit error rate performance is affected when the two resonators have mismatched resonant frequencies, because the mismatch will reduce the bandwidth tremendously when the two antennas both have very high Q factor.

Based on the review, almost all groups are transmitting data digitally, whether in a separated channel or in a unified channel. However, to digitize a signal requires a complicated circuit design, so in this thesis we propose to use asynchronous sigma-delta modulation to process the data into a two-level analog signal, so that the circuit design can be simplified.

2.3 THEORETICAL TOOLS FOR ANALYSING WPT SYSTEMS

2.3.1 Coupled mode theory (CMT)

In the 1950's, Miller and Pierce developed the CMT to study the microwave transmission lines and electron beams problem. This theory was then generalized to analyze a large number of problems in microwave waveguide and optoelectronic area. There are many possible modes in a RF device, for example a microwave waveguide, and the CMT is to analyze a coupled system by handling the modes of the uncoupled system. Schelkunoff gave a rigorous derivation of CMT, showing that if a complete set of modes is used, the CMT is equivalent to Maxwell's equations. However, in most cases, only the first one or two modes are used, so the CMT is still an approximation [31]. In the case of magnetic resonant coupling WPT, only the lowest order modes are considered, which the natural frequencies of those resonators are. This assumption is only accurate for resonators with high quality factors where the fundamental frequency of the resonator is much larger than the bandwidth and can be modeled as a simple RLC circuit around the resonant frequency with high accuracy. And fortunately, people always use high Q resonators in a WPT system for the sake of efficiency. In this section, the CMT is introduced in detail. Figure 7 shows an LC circuit, which is the equivalent circuit of a lossless resonator around its lowest resonant frequency. Here the voltage on the capacitor and the current across the inductor are selected as the state variable to describe the circuit and we can write the following state space equations:

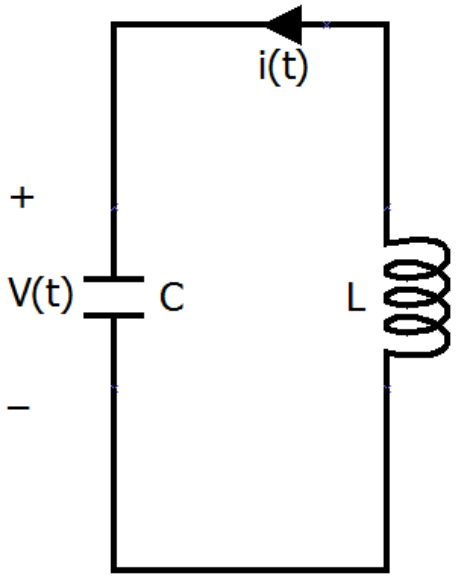

Figure 7. LC tank

$$i = C\frac{dv}{dt} \qquad (2.1)$$

$$v = -L\frac{di}{dt}$$

To simplify the analysis, a decoupling is performed and the decoupled variables can be calculated as:

$$a_{\pm} = \sqrt{\frac{C}{2}}v \pm j\sqrt{\frac{L}{2}}i \qquad \textbf{(2.2)}$$

This way, the new state equations are:

$$\dot{a}_{\pm} = \pm j\omega_0 a_{\pm} \qquad \textbf{(2.3)}$$

where $\omega_0 = \frac{1}{\sqrt{LC}}$ $\omega_0 = \frac{1}{\sqrt{LC}}$ is the natural frequency of the resonator, a_+ and a_- are known as positive and negative frequency components respectively. As shown in (2.3), these two equations

are complex conjugations of each other, so either one of them is enough to totally describe the system, and the author chose to use the equation of a_+ a_+, and will ignore the plus sign from now on. Another important property of these frequency components is that $|a_\pm|^2$ $|a_\pm|^2$ equals the energy stored in the resonator. This can be verified by directly solve (2.1), and the solution is:

$$\begin{aligned} v &= V\sin(\omega_0 t+\theta) \\ i &= CV\omega_0\cos(\omega_0 t+\theta) \end{aligned} \qquad \textbf{(2.4)}$$

Plugging (2.4) into the definition of a_+, we get

$$a=\sqrt{\frac{C}{2}}Ve^{j(\omega_0 t+\theta)} \qquad \textbf{(2.5)}$$

So

$$|a|^2=\frac{C}{2}V^2=E \qquad \textbf{(2.6)}$$

Until now we have been talking about lossless resonators, and if there is loss, the state equations can be modified to

$$\dot{a}=j\omega_0 a-\Gamma_0 a \qquad \textbf{(2.7)}$$

where Γ_0 is the intrinsic loss rate of the resonator. And it should be noted that (2.7) is an approximation for resonators with small loss, which is another assumption in CMT.

Now we are getting to the coupling between two resonators, denoted as resonator 1 and 2 with the positive frequency components a_1 and a_2. The differential equations governing this system are

$$\dot{a}_1 = (j\omega_1 - \Gamma_1)a_1 + j\kappa_{12}a_2$$
$$\dot{a}_2 = (j\omega_2 a_2 - \Gamma_2)a_2 + j\kappa_{21}a_1 \quad \textbf{(2.8)}$$

where κ_{12} κ_{12} and κ_{21} κ_{21} are known as coupling coefficients.

(2.8) is similar to what we found in one resonator case except for those coupling terms. People may expect the $\kappa's$'s to be linear integrodifferential operators, however in the situation when $|\kappa_{12}a_2|$ $|\kappa_{12}a_2|$ is much smaller than $|(j\omega_1 - \Gamma_1)a_1|$ $|(j\omega_1 - \Gamma_1)a_1|$, the coupling will affect the time evolution of a_1 and a_2 only when ω_1 is similar to ω_2, in which case the time dependence is approximately in the form of $e^{j\frac{\omega_1+\omega_2}{2}t}$, so both integral and differential operators are equivalent to multiplying a complex number [32].

Now we have set up the formula and explained all the parameters we need to analyze a magnetic resonant coupling WPT system, so in the next part a two resonator witricity system will be taken as an example to show how to apply the CMT to analyze it.

A two-resonator witricity system has one transmitting resonator, which is inductively coupled with a source loop, and one receiving resonator, which is inductively coupled with a load loop, so the system setup is like what is shown in Figure 6. The differential equations describing the system can be written as

$$\dot{a}_1 = (j\omega_1 - \Gamma_1)a_1 + j\kappa a_2 + f$$
$$\dot{a}_2 = (j\omega_2 a_2 - \Gamma_2 - \Gamma_W)a_2 + j\kappa a_1 \quad \textbf{(2.9)}$$

where a_1 a_1 and a_2 a_2 are the positive frequency components in the transmitting resonator and receiving resonator respectively; Γ_1 and Γ_2 are the intrinsic loss of each resonator and Γ_W

represents the effective load coupled with the receiving resonator; κ is the coupling coefficient between these two resonators, which is a real number; and f is the input coupled with the transmitting resonator.

Optimal conditions to get maximal efficiency are derived here to show the application of CMT on a WPT system. The physical definition of efficiency is the ratio of power on the load out of the total power supplied to the system, and this can be written as the following equation:

$$\eta = \frac{2\Gamma_W |a_2|^2}{2\Gamma_1 |a_1|^2 + 2(\Gamma_W + \Gamma_2)|a_2|^2} \tag{2.10}$$

The numerator is the power consumed on the load and the denominator is the total power consumption of the whole system, so the equation for efficiency is consistent with the physical definition. After some algebraic deduction, (2.10) becomes

$$\eta = \frac{\Gamma_W \left|\frac{a_2}{a_1}\right|^2}{\Gamma_1 + (\Gamma_W + \Gamma_2)\left|\frac{a_2}{a_1}\right|^2} \tag{2.11}$$

(2.11) shows that $\left|\frac{a_2}{a_1}\right|^2$ $\left|\frac{a_2}{a_1}\right|^2$ is important to calculate the efficiency. This term can be found using (2.9). If we drive the system by a source with frequency ω_0 ω_0, in steady state both a_1 and a_2 have a time-dependent term $e^{j\omega_0 t}$, then the second equation in (2.9) becomes

$$(\Gamma_2 + \Gamma_W)a_2 = j\kappa a_1 \tag{2.12}$$

where $\left|\frac{a_2}{a_1}\right|^2$ $\left|\frac{a_2}{a_1}\right|^2$ can be calculated and the steady state efficiency would be

$$\eta_s = \frac{\frac{\Gamma_W}{\Gamma_2}\frac{\kappa}{\Gamma_1\Gamma_2}}{\left(1+\frac{\Gamma_W}{\Gamma_2}\right)^2 + \left(1+\frac{\Gamma_W}{\Gamma_2}\right)\frac{\kappa^2}{\Gamma_1\Gamma_2}} \tag{2.13}$$

Now, to maximize the efficiency, we first set $\frac{\partial \eta_s}{\partial \Gamma_W} = 0$ $\frac{\partial \eta_s}{\partial \Gamma_W} = 0$, and the optimal load we get is

$$\Gamma_{W,opt} = \sqrt{\Gamma_2^2 + \kappa^2 \frac{\Gamma_2}{\Gamma_1}} \tag{2.14}$$

where Γ_1 Γ_1, Γ_2 Γ_2 and κ are parameters decided only by the resonators and their relative position, so we consider them as constants for a given system. To prove that the obtained extremum is a maximum, we inspect (2.13), which shows that when $\Gamma_W \to 0$ $\Gamma_W \to 0$ and $\Gamma_W \to +\infty$, the efficiency on both case are zero. Known the fact that efficiency is always a positive number, we can assert that the only extremum we found is a global maximum. With the optimal load, we get the maximized steady state efficiency

$$\eta_{s,\max} = \frac{\frac{\kappa^2}{\Gamma_1\Gamma_2}}{\left(1+\sqrt{1+\frac{\kappa^2}{\Gamma_1\Gamma_2}}\right)^2} \tag{2.15}$$

(2.15) shows that $\frac{\kappa^2}{\Gamma_1\Gamma_2}$ $\frac{\kappa^2}{\Gamma_1\Gamma_2}$ is a key term to determine the optimal efficiency, hence it is known as the figure of merit of this system. When the figure of merit is much greater than 1, the system

can get high efficiency. In a typical magnetic resonant WPT system κ is much smaller than 1, so the system requires small loss or high Q factor to achieve high efficiency. From this example, we can see that CMT is a handy tool to analyze a magnetic resonant coupling WPT system.

To sum up, CMT is a linear approximation of the real system, which not only greatly simplified the analysis of a WPT system compared to using electromagnetics method but also reduced the number of differential equations required to describe the circuit by half compared to the circuit theory. However, for the approximation to be accurate, the CMT made several assumptions: (1) high Q factor assumption. The quality factor of both the transmitter and the receiver resonators should be much larger than 1, so that the resonator can be modeled as an RLC tank and the loss term in the formulas can be legally expressed as a linear term. (2) Resonance assumption. The resonant frequencies of the transmitter and receiver must be similar. (3) Weak coupling assumption. The coupling factor κ κ between the transmitter and receiver should be much smaller than the resonant frequencies ω_1 ω_1 and ω_2 . Assumption (2) and (3) together guarantee that the coupling term is also linear in the formula. These assumptions, while are normally satisfied in a magnetic resonant WPT system, will fail the screening in some cases, e.g. when the two resonators are too close to each other or when we deliberately make the coils off resonant for data transmission as in the RFID case. Another limitation of the CMT method is that the parameters in the formulas, e.g. a_+, a_+, κ and Γ are not physical parameters but are mathematically defined, while this makes the analysis of the system easier, the physical meaning of the parameters are not clear any more, also the measurement of these parameters is not as intuitive as measuring physical parameters, such as resistance, capacitance and inductance.

2.3.2 Equivalent circuit model (ECM)

The equivalent circuit model, compared to the CMT, is more familiar to electrical engineers, which uses lumped elements to model the resonators. To model an RF component using lumped elements is not always possible. However for resonators with high Q factors, where the frequency difference between neighboring resonant peaks is much larger compared to the bandwidth of those peaks, we can use a simple RLC tank to approximate the resonator when the frequency is lower than the second resonant frequency. This approximation can provide accurate results as shown in many research works listed at the beginning of this chapter. To compare with the CMT method, a two-resonator witricity system, which is the same as in the previous section, will be analyzed in this section using the equivalent circuit method.

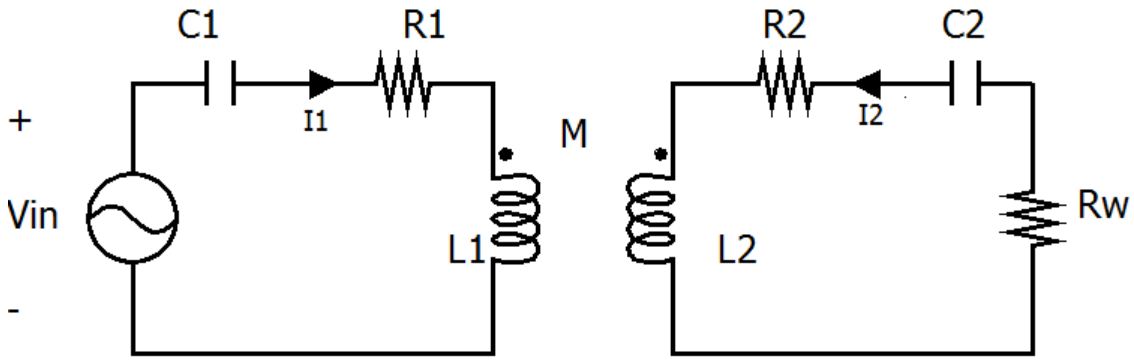

Figure 8. Equivalent circuit of a two-resonator magnetic resonant coupling WPT system

The equivalent circuit of a two-resonator magnetic resonant coupling WPT system is shown in Figure 8, for easy of analysis and to make the situation comparable to the CMT case, the two single loops in the system were ignored and the source and load are directly connected to the resonators. Using KVL, we get the following equations:

$$\begin{bmatrix} R_1 + j\omega L_1 & j\omega M \\ j\omega M & R_2 + R_W + j\omega L_2 + \dfrac{1}{j\omega C_2} \end{bmatrix} \begin{bmatrix} I_1 \\ I_2 \end{bmatrix} = \begin{bmatrix} V_{in} \\ 0 \end{bmatrix} \quad \textbf{(2.16)}$$

where the RLC's are resistances, inductances and capacitances of the transmitting and receiving resonators respectively, M is the mutual inductance between the two resonators, the I's are the currents in resonators with flowing directions shown in the figure and V_{in} is the voltage supplied to the transmitter. To simplify the representation of the equation, I will denote $j\omega L_i + \dfrac{1}{j\omega C_i}$ $\mathbf{j\omega L_i + \frac{1}{j\omega C_i}}$ as $\mathbf{jX_i}$, which represents the reactance of the corresponding resonator.

(2.16) can be solved by inversing the coefficient matrix and the result is:

$$\begin{aligned} I_1 &= \frac{(R_2 + R_W + jX_2)V_{in}}{R_1(R_2 + R_W) - X_1X_2 + \omega^2M^2 + j[R_1X_2 + (R_2 + R_W)X_1]} \\ I_2 &= \frac{-j\omega MV_{in}}{R_1(R_2 + R_W) - X_1X_2 + \omega^2M^2 + j[R_1X_2 + (R_2 + R_W)X_1]} \end{aligned} \quad \textbf{(2.17)}$$

The efficiency can be expressed as

$$\eta = \frac{|I_2|^2 R_W}{real\{V_{in}I_1^*\}} \quad \textbf{(2.18)}$$

Plugging (2.17) into (2.18), we get

$$\eta = \frac{\omega^2M^2R_W}{R_1(R_2 + R_W)^2 + (R_2 + R_W)\omega^2M^2 + X_2^2R_1} \quad \textbf{(2.19)}$$

Define the denominator as $\mathbf{D(X_1, X_2)}$, and we can minimize D to maximize the efficiency. Clearly, D is maximized when $\mathbf{X_2 = 0}$, which means the system is driven at the resonant frequency of the receiving resonator, and the efficiency becomes

$$\eta|_{X_2=0} = \frac{\omega^2 M^2 R_W}{R_1(R_2+R_W)^2 + (R_2+R_W)\omega^2 M^2} \tag{2.20}$$

To find the optimal load, we set $\frac{\partial \eta|_{X_2=0}}{\partial R_W} = 0$ $\frac{\partial \eta|_{X_2=0}}{\partial R_W} = 0$ and solve for the load

$$R_{W,opt} = \sqrt{\frac{R_2}{R_1}\omega^2 M^2 + R_2^2} \tag{2.21}$$

To make sure that the obtained load is optimal, usually we need to verify that the second derivative is positive. However, here by inspecting (2.20), we find that the efficiency is always positive and goes to 0 when R_W goes to 0 or $+\infty$ $+\infty$, so the only extremum we found have to be a maximum point. Hence the optimal efficiency is

$$\eta_{opt} = \frac{\frac{\omega^2 M^2}{R_1 R_2}\sqrt{\frac{\omega^2 M^2}{R_1 R_2}+1}}{\left(2+\frac{\omega^2 M^2}{R_1 R_2}\right)\left(1+\sqrt{\frac{\omega^2 M^2}{R_1 R_2}+1}\right)} \tag{2.22}$$

Comparing this result with the one we got with CMT, we can see that certain connection exists between Γ and R as well as between κ and ωM, which is consistent with the definition of those parameters, as both Γ and R are related to the intrinsic loss of the resonators while κ and ωM are both coupling factors. With that known, we can see that both CMT and EQC give same result for optimal load value, while the equation for maximum efficiency from EQC is much more complex than the result we got from CMT. However a deeper inspection shows that the equation from CMT is nothing but an approximation of the EQC result when $\frac{\kappa^2}{\Gamma_1\Gamma_2} \gg 1$.

2.3.3 Pros and cons of ECM and CMT methods

From the above analysis, we can conclude that both CMT and ECM are linear approximations of a real WPT system, and ECM is a better than CMT when considering the accuracy, because CMT makes stronger assumptions than ECM. While CMT has the advantage of reducing the order of the system by half and thus is a more concise expression, the mathematical operations made on the state variables to achieve this advantage make the physical meanings of the new state variables not as clear as in the ECM and more difficult to measure. So in this work, the transfer function of the WPT system will be derived from equivalent circuit model. From the previous examples, we can see that for a simple two-resonator system, both methods give elegant results, however we can also imagine that these procedures are hard to repeat for a system with very large number of resonators, in which case even if we can solve for the expression of efficiency, the optimization will be a problem for such a complicated objective function and so many variables. So, pure analytical methods are difficult to apply in a multiple-resonator system and a pure finite element method will take too much time and resource to do the analysis, and a semi-analytical method is needed, which is the main purpose of this dissertation. Also, in the previous examples, no spatial information is included in the analysis, so we will never know how to arrange the resonators so that the maxima of a certain cost function can be achieved. The parameter that connects the electronics behavior of the system and the position information is the mutual inductance, and a detailed analysis of this parameter will also be included in this work.

2.4 REVIEW OF TOOLS FOR DATA TRANSMISSION

2.4.1 Asynchronous sigma-delta modulation (ASDM)

Developed decades ago, ASDM has just begun to gain its popularity in the electronic field as a method of A/D conversion, or more precisely, to convert analog signal to a pulse train with varying width. ASDM has very simple circuit and does not require a clock signal to operate, so that it consumes less power than the traditional methods. A typical circuit model of ASDM is shown in Figure 9, which shows that the circuit only consists of an integrator and a Schmitt Trigger. In ASDM analog signal is converted to pulse train with only two voltage levels as shown in the right part of Figure 9, and all the information is stored in the zeros-crossing times, i.e. original signal can be recovered if zeros-crossing information is given. A brief explanation of how this circuit works is given below [34, 35].

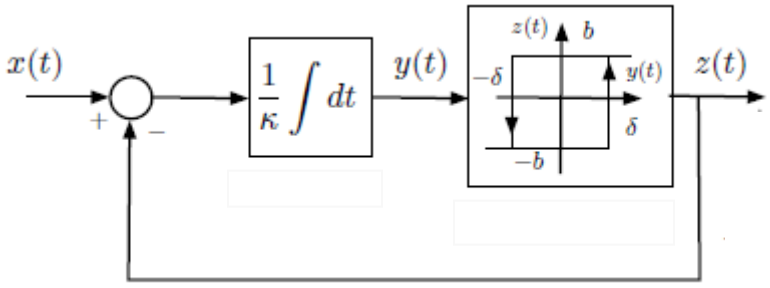

Figure 9. Asynchronous sigma delta modulator

Assuming that a bounded and band-limited signal $x(t)$, with maximum frequency f_{max} and maximum amplitude $c \leq b$, is fed into the circuit. We can see that the output from the integrator $y(t)$ is

$$y(t) = y(t_0) + \frac{1}{\kappa}\int_{t_0}^{t} [x(\tau) - z(\tau)]d\tau \tag{2.23}$$

Since $c < b$, we can see that the sign of $x(\tau) - z(\tau)$ totally depends on $z(\tau)$. Without loss of generosity, we assume that $z(t_0) = -b\, z(t_0) = -b$, so that $x(\tau) - z(\tau) > 0$ and $y(t)$ is increasing over time until time t_1 when $y(t)$ reaches the upper trigger level δ and $z(\tau)$ becomes b so that $y(t)$ starts decreasing till it reaches the lower trigger level $-\delta$ at t_2 and one cycle is finished. With the above explanation, we get a general equation describing the behavior of this circuit

$$\int_{t_k}^{t_{k+1}} x(\tau)d\tau = (-1)^k \left[-b(t_{k+1} - t_k) + 2\kappa\delta\right] \tag{2.24}$$

Where t_k's are the zero-crossing times subscribed by the order of occurrence. Intuitively, given the adjacent zero-crossing times t_k and t_{k+1} we get the average value of x in between, and when the zero-crossing happens frequent enough, we expect to have a perfect recovery of the input signal. A more rigorous condition for perfect recovery is stated as

$$\max_k (t_{k+1} - t_k) < T_N \tag{2.25}$$

where T_N is the Nyquist sampling period.

To choose the parameters b, δ, and κ, we need to go back to equation (2.24), where by applying the mean value of theorem to the left-hand-side integral, we get

$$(t_{k+1} - t_k)x(\xi) = (-1)^k \left[-b(t_{k+1} - t_k) + 2\kappa\delta \right] \tag{2.26}$$

where ξ is somewhere between t_{k+1} and t_k. With the assumption that x is bounded by constant c, we get a bound of the time duration

$$\frac{2\kappa\delta}{b+c} \le t_{k+1} - t_k \le \frac{2\kappa\delta}{b-c} \tag{2.27}$$

So, the condition for perfect recovery on κ, δ, and b is

$$\frac{2\kappa\delta}{b-c} \le T_N \tag{2.28}$$

The proof for perfect recovery is somewhat complex and is not the main concern of this dissertation, so I will only show the algorithm to recovery the original signal from the sequence of time stamps of zero-crossings. Firstly, some auxiliary vectors and matrices are defined by

$$\begin{aligned} \vec{g} &= \left[g(t - s_k) \right] \\ \vec{q} &= \left\{ (-1)^k \left[2kd - b(t_{k+1} - t_k) \right] \right\} \\ \underline{\underline{G}} &= \left[G_{lk} \right] = \left[\int_{t_l}^{t_{l+1}} g(\tau - s_k) d\tau \right] \end{aligned} \tag{2.29}$$

where g(.) is the sinc function, and s_k is the average of t_k and t_{k+1} [35]. Now the original signal can be recovered by

$$x(t) = \vec{g}^T \underline{\underline{G}}^+ \vec{q} \tag{2.30}$$

Now a simple simulation is performed to show the performance of this mechanism, where the input is created by summing up 3 sinusoidal waves with randomly generated frequencies bounded by a preselected maximum frequency. The result is shown below

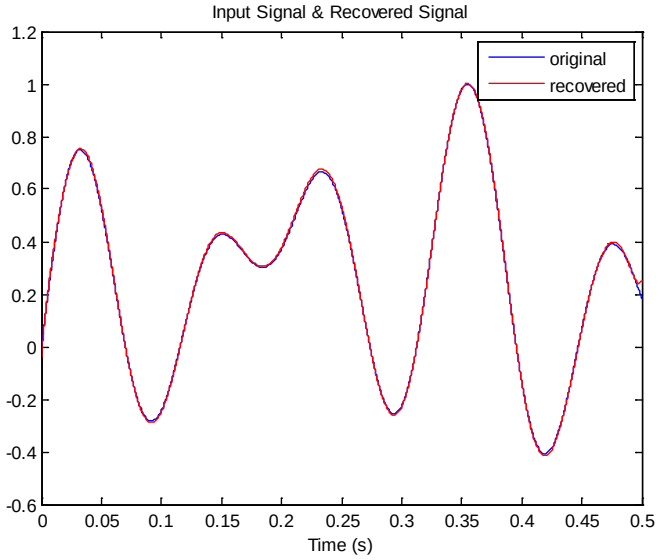

(a)

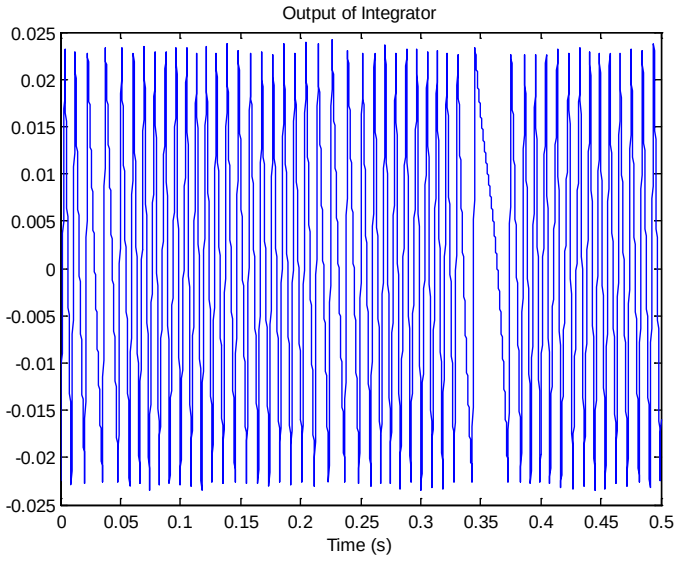

(b)

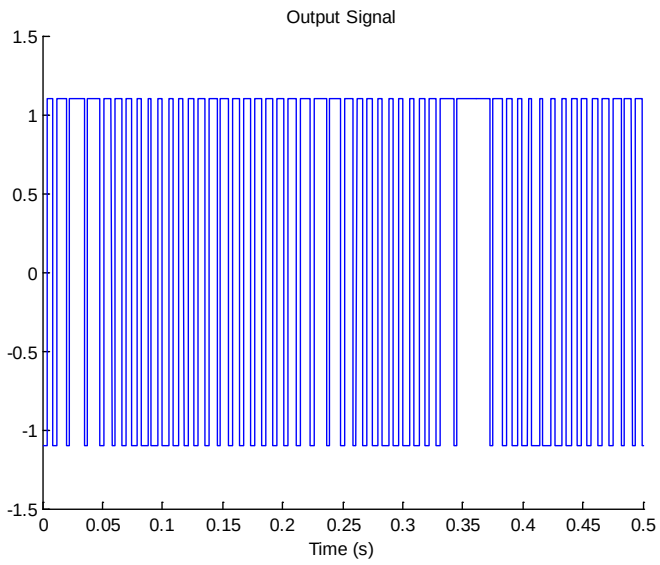

(c)

Figure 10. Simulated encode and decode results from ASDM.

The maximum frequency and the amplitude of the input signal is 10 Hz and 1, respectively. The parameters of the modulator are: b=1.1, $\delta = 0.0225$, $\kappa = 0.1$. (a)The original and recovered signal. (b) the output from integrator in the modulator. (c) the output of the modulator.

The parameters of the modulator are chosen such that the condition for perfect recovery is satisfied. And from the simulation results, we can see that the recovered signal traces the original signal well, even though there is a short deviation at the end of the simulation due to the reason that the last switch of the Schmitt trigger has not arrived yet.

As the output from an ASDM system has only two voltage levels, it is suitable to transmitted using load modulation, which will be reviewed in the next section.

2.4.2 Load Modulation

Load Modulation, as used in passive RFID tags, is a widely used method for backward data transmission [36]. As indicated by the name, this method is an application of the phenomena that the change of load of the secondary coil of a coupled system will be reflected in the primary side. Thus, by adjusting the load value according to the signal to be transmitted, the backward data transmission is achieved. The structure of a load modulation system is shown in Figure 11 and the data can be modulated on the carrier by changing load on the receiver side of the wireless power transfer system as in Figure 12, where the red line marks the time when the load changes status.

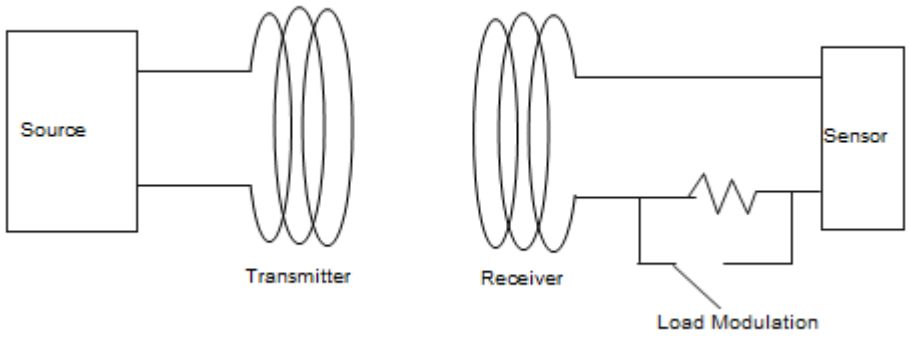

Figure 11. Sketch of load modulation system

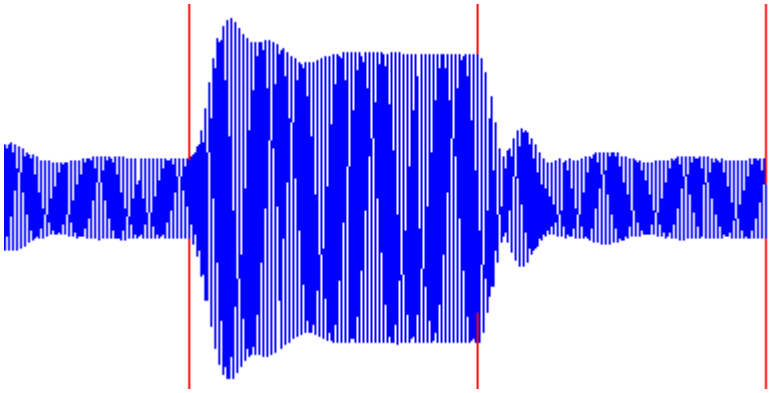

Figure 12. Example of a load modulated signal

2.4.3 Summary

With ASDM and load modulation, a simply signal channel can be built to transmit data to the power transmitter. By the nature of ASDM, clock is not necessary as the signal to be transmitted is analog, and a multiplier is also unnecessary for the purpose of modulation. Both these characteristics greatly reduced the power consumption and complexity of the data transmission system. One drawback of this idea of integrating data transmission function into power transmission channel is that the data rate is limited by the low carrier frequency and high quality factor characteristics of the magnetic resonant power transmission system. So a model-referenced data recovery algorithm will be developed in the later part to make better use of the data channel.

3.0 TRANSFER FUNCTION BASED MULTI-RESONATOR WPT SYSTEM DESIGN

From the previous chapters, we know that a design method for system with large number of resonators is needed. So in this part, I will introduce the proposed method for optimizing the design based on transfer function and will use an example to show the design procedure. However, as stated at the end of the last chapter, without a good understanding of the relationship between the spatial arrangement of the coils and the mutual inductance between them, we cannot get the optimized arrangement. Even if we only want to optimize the mutual inductance, it is difficult for a multiple-resonator system because all the mutual inductance is dependent on each other and cannot be optimized separately. So the most important task of optimizing a multiple-resonator system is to understand the how the spatial arrangement of two resonators will affect the mutual inductance between them. After getting this relation, we can substitute the mutual inductance in transfer function as a function of distance and optimize the positions of resonators to achieve maximum transfer function.

3.1 METHODS

3.1.1 Equivalent circuit and transfer function

In this and the following sections, I will use 3-coil relayed system as an example to show how the transfer function based method will work for designing a multiple resonator system. A relayed WPT system is shown in Figure 13, where a relay coil is inserted between the transmitter and receiver. This kind of setup has been proposed several years ago to increase the effective transmission range of a WPT system; however, the proper position of the relay coil hasn't been well decided. So in this example, I will use the proposed method to find the optimal position of the relay resonator.

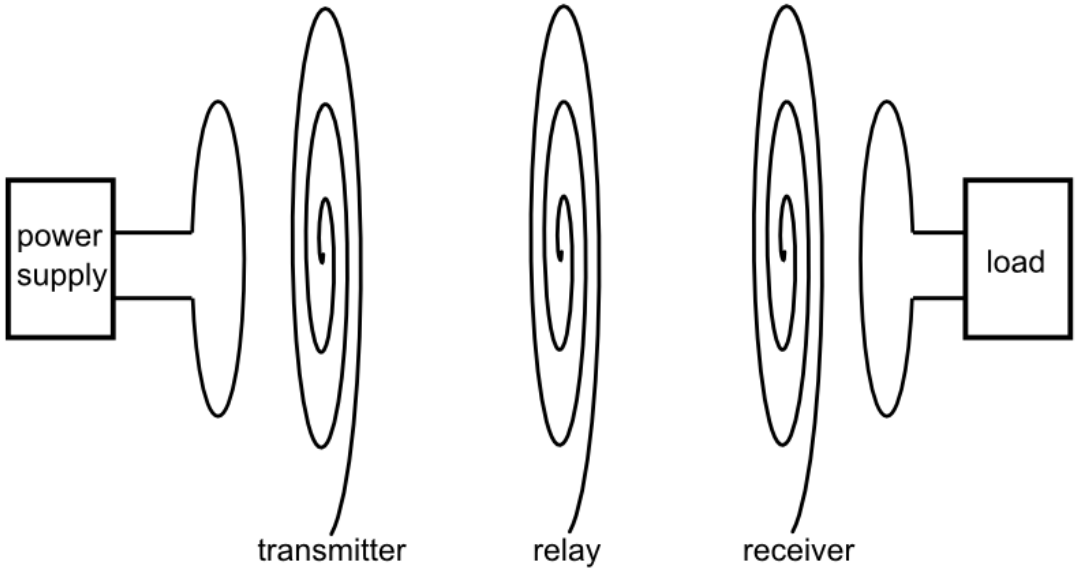

Figure 13. Sketch of a WPT system with relay

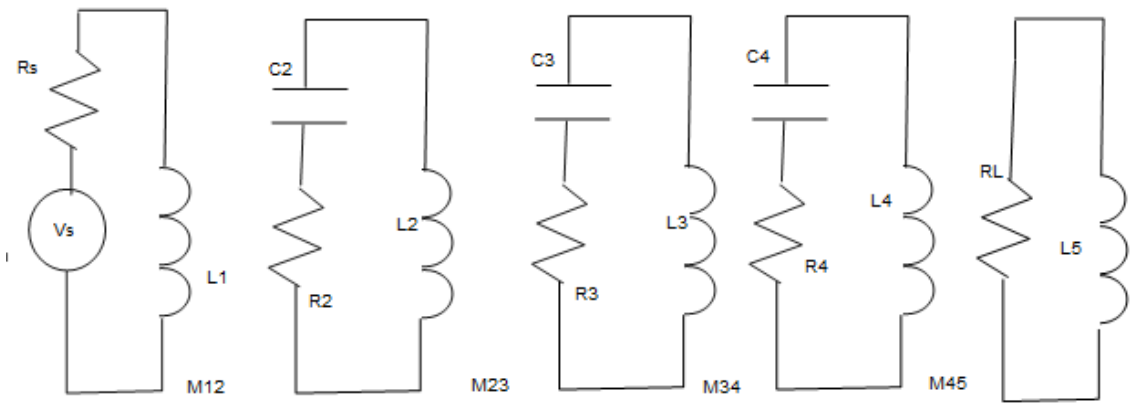

Figure 14. Equivalent circuit of a relayed magnetic resonant wireless power transmission system

As stated before, the transfer function will be derived from the equivalent circuit model which is shown in Figure 14. In this circuit, we only consider the coupling between adjacent resonators and loops, as they are larger than the coupling between nonadjacent ones.

From Kirchhoff's voltage law, we can write the following equations and derive the transfer function from them.

$$\begin{aligned} V_S &= I_1 Z_1 + sM_{12} I_2 \\ 0 &= I_2 Z_2 + sM_{12} I_1 + sM_{12} I_3 \\ 0 &= I_3 Z_3 + sM_{23} I_2 + sM_{23} I_4 \\ 0 &= I_4 Z_4 + sM_{34} I_3 + sM_{45} I_5 \\ 0 &= I_5 Z_5 + sM_{45} I_4 \end{aligned} \qquad \textbf{(3.1)}$$

Here Z_i $\boldsymbol{Z_i}$ is the loop impedance of the i[th] coil, $\boldsymbol{M_{ij}}$ is the mutual inductance of the i[th] and j[th] resonator. To solve for the transfer function, we first express the previous equation in matrix form :

$$\begin{bmatrix} V_S \\ 0 \\ 0 \\ 0 \\ 0 \end{bmatrix} = \begin{bmatrix} Z_1 & sM_{12} & & & \\ sM_{12} & Z_2 & sM_{23} & & \\ & sM_{23} & Z_3 & sM_{34} & \\ & & sM_{34} & Z_4 & sM_{45} \\ & & & sM_{45} & Z_5 \end{bmatrix} \begin{bmatrix} I_1 \\ I_2 \\ I_3 \\ I_4 \\ I_5 \end{bmatrix} \quad \textbf{(3.2)}$$

The current in the load loop, I_5, can be calculated using Cramer's rule

$$I_5 = \begin{vmatrix} Z_1 & sM_{12} & & & \\ sM_{12} & Z_2 & sM_{23} & & \\ & sM_{23} & Z_3 & sM_{34} & \\ & & sM_{34} & Z_4 & \\ & & & sM_{45} & \end{vmatrix} V_S \Big/ \begin{vmatrix} Z_1 & sM_{12} & & & \\ sM_{12} & Z_2 & sM_{23} & & \\ & sM_{23} & Z_3 & sM_{34} & \\ & & sM_{34} & Z_4 & sM_{45} \\ & & & sM_{45} & Z_5 \end{vmatrix} \quad \textbf{(3.3)}$$

And the transfer function can be calculated as

$$G(s) = I_5 R_L / Vs \quad \textbf{(3.4)}$$

There are several parameters in this transfer function that depend on a specific coil design, e.g. self-inductance, series resistance et al. So in the next step, these parameters will be extracted experimentally for our resonator.

3.1.2 Resonator Design and Parameter Measurement

A famous result from functional analysis shows that, among all the shapes, circle has the smallest circumference-to-area ratio. As the Q factor of a inductor can be calculated as $\omega L/R$,

where the inductance L is positive correlated with the area enclosed by the inductor, and the series resistance R is proportional to the length of wire, so solenoid has been known as having the best Q factor. However, with the 3D structure, the manufacture of a solenoid is not as easy as a printed board. Besides, the large volume of a solenoid makes it not suitable for certain

applications, e.g. implantable devices. So in our design a spiral resonator is used, which is shown in Figure 15. This design keeps the circular shape for higher Q factor while compressed into a single plane for easier manufacture and smaller volume. The resonator is a regularly hexagonal PCB with a printed spiral coil, 14cm in diameter, 3mm in trace width with a 1.5mm trace spacing. The total number of turns is 15. Several metal pieces are put on the back to increase the parasitic capacitance and thus to decrease the resonant frequency.

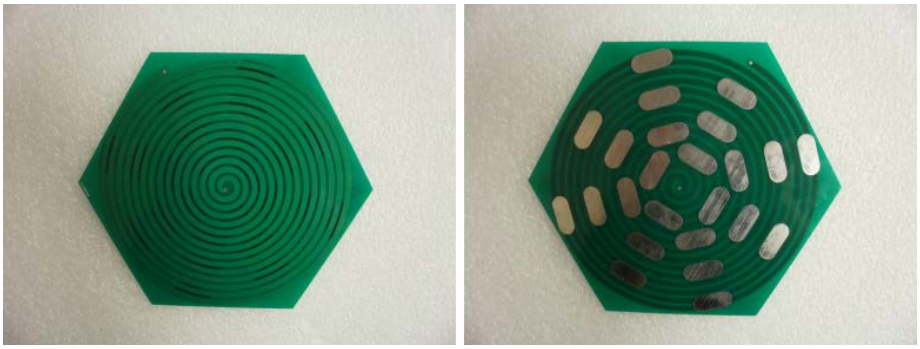

Figure 15. Resonator used in the experiments

The resonator can be modeled as a lousy inductor connected in parallel with a stray capacitance, as shown in Figure 16, where the parameters can be measured using a network analyzer.

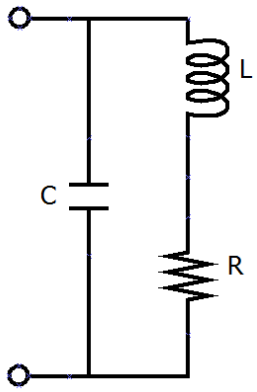

Figure 16. Circuit model of a spiral resonator

The impedance of this circuit is:

$$H(\omega) = \frac{R + j\omega L}{1 - \omega^2 LC + j\omega RC} \tag{3.5}$$

There are several definitions of resonance, e.g. when the impedance is purely resistive or when the magnitude of the impedance reaches its maximum. Fortunately, for a high Q resonator, these definitions all lead to similar resonant frequency, and in this work I use the frequency with maximum impedance as resonant frequency, when $\omega^2 LC = 1$. And the Q factor of this circuit can be calculate as

$$Q = \frac{f_0}{f_1 - f_2} \tag{3.6}$$

where f_0 is the resonant frequency or the frequency where the maximum magnitude of impedance is achieved. And f_1 , f_2 are the frequencies, where the magnitude of impedance is 0.707 times of the maximum value. Thus, from the measured curve of impedance, both the resonant frequency and the Q factor of a coil can be determined. To determine the RLC values of the resonator, we first examine equation (3.4), where the equivalent resistance R_s at resonance is L/RC. With this known, the RLC values can be calculated from the following equations:

$$\begin{aligned} R_S &= L / RC \\ Q &= \omega_0 L / R \\ \omega_0 &= 1/\sqrt{LC} \end{aligned} \tag{3.7}$$

The measurement was performed using a network analyzer and the setup is shown in Figure 17. The network analyzer was calibrated at the output port, due to the limitation of the

standard calibration kit. Fortunately, the cable connecting the port to the device under test is short compared to the wave length (>10m), so the influence of cable can be ignored. Before the measurement, the impedance of the probe itself was measured first and the result shows that the magnitude of impedance around resonant frequency is about 18, which is much smaller compared to the impedance of the resonator (in the order of 10^4) and can be safely ignored.

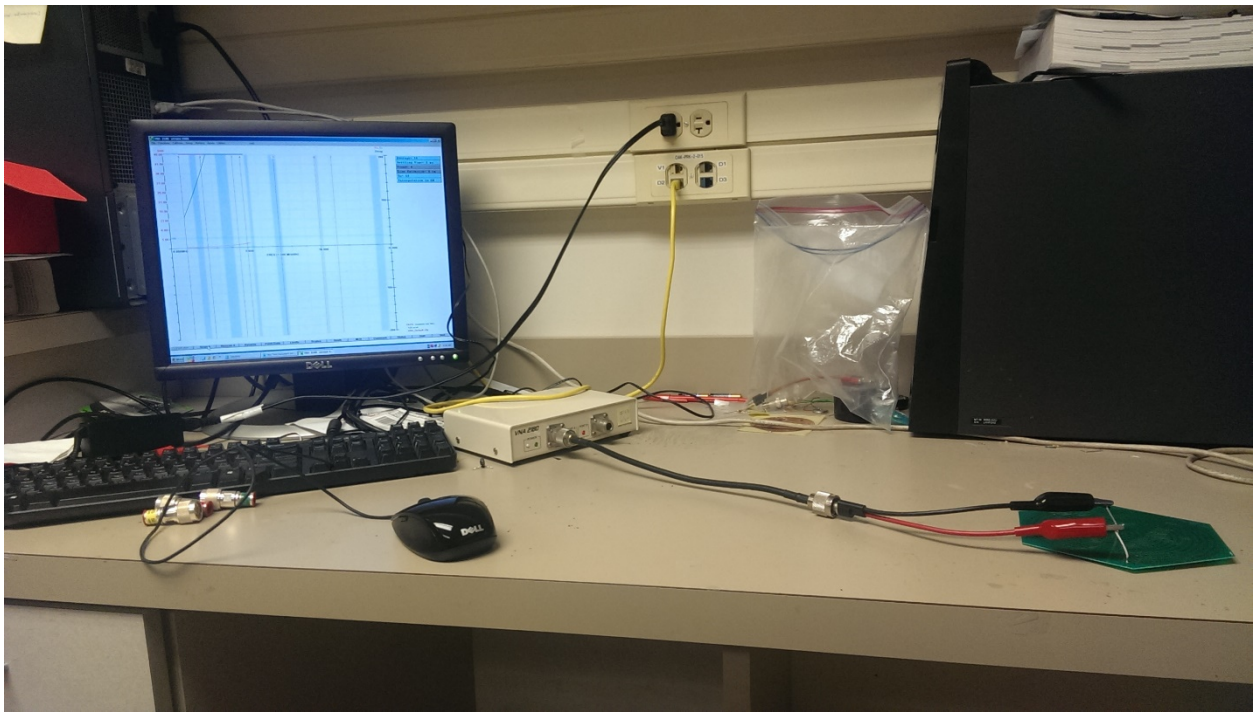

Figure 17. Experimental setup for measuring coil parameters

Each of the three resonators were measured 5 times and the result is shown in Table 1.

Table 1. Parameters of Resonators

	f_0(MHz)	Q	R(Ohm)	L(uH)	C(pF)
1	8.384±0.043	82.2±6.9	6.41±0.99	9.9±0.63	36.5±2.5
2	8.455±0.024	89.3±8.9	6.29±0.98	10.4±0.69	34.0±2.3
3	8.382±0.014	87.6±7.1	5.67±0.77	9.4±0.56	38.6±2.3

The measured impedance matches the impedance of the circuit model well as shown in Figure 18, which proves that a high Q resonator can be modeled as a simple RLC tank near the resonant frequency.

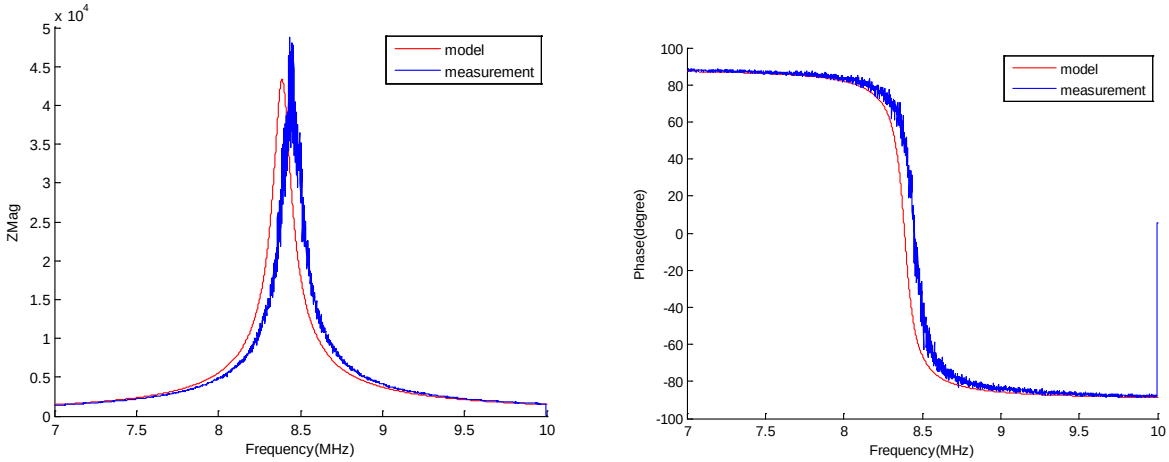

Figure 18. Impedance of the circuit model vs a measured impedance of the first resonator

3.1.3 Mutual Inductance Analysis

Mutual inductance is a measure of how much coupling exists between two metals, so in this section we only analyze the mutual inductance between two resonators. However, we needed

firstly answer the question whether analyzing mutual inductance pairwisely is feasible, because any extra pieces of metal in a system will affect the distribution of magnetic field in the space. To answer this, we need to know that metal pieces will alter the magnetic field in two ways. Firstly ferromagnetic materials will affect the magnetic field distribution without generating any macro current. If this happens, we cannot ignore its influence on the mutual inductances between other pairs of metals. Fortunately in our system, the resonators are copper, which is not ferromagnetic. And the second way a conductor will affect the magnetic field distribution is by generating inductive currents. This effect will not affect our analysis result if every pair of mutual inductances is included in the equations as mutual inductance governs the induced current. Thus we conclude that it is feasible for us to analyze mutual inductance pairwisely. The mutual inductance can be calculated from Neumann formula:

$$M_{ij} = \frac{\mu_0}{4\pi} \oint_{C_i} \oint_{C_j} \frac{d\vec{s}_i \cdot d\vec{s}_j}{\left|\vec{R}_{ij}\right|} \tag{3.8}$$

In our case, we use spiral resonators, which can be approximated by a set of concentric circles, as shown in Figure 19.

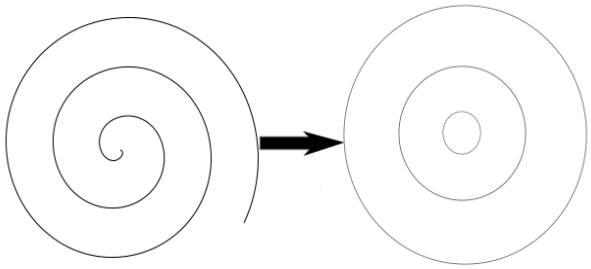

Figure 19. Concentric loops model of a circular coil

As superposition holds for Neumann formula, we will first analyze the mutual inductances of a pair of single loops, which can be generalized into multiple-loop resonators in later work.

3.1.3.1 Mutual inductance between two loops

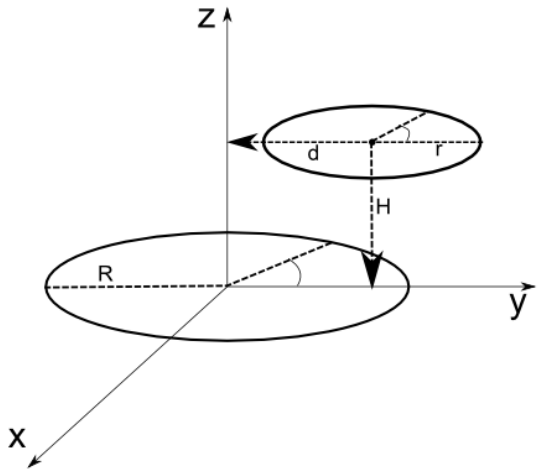

Figure 20. Sketch of two wire loops with lateral misalignment

As show in Figure 20, we have a circle with radius R, centered at origin and perpendicular to z axis. The radius of the other circle is r, the separation between two circles is D and the amount of lateral misalignment is d. Based on this setup, we have

$$\boldsymbol{r_1} = -R\sin\phi_1 \boldsymbol{a_z} + R\cos\phi_1 \boldsymbol{a_y}$$

$$\boldsymbol{r_2} = -r\sin\phi_2 \boldsymbol{a_x} + (d + r\cos\phi_2)\boldsymbol{a_y} + H\boldsymbol{a_z} \quad \textbf{(3.9)}$$

$$d\boldsymbol{s_1} = R\left(-cos\phi_1 \boldsymbol{a_x} - sin\phi_1 \boldsymbol{a_y}\right)d\phi_1$$

$$d\boldsymbol{s_2} = r\left(-cos\phi_2 \boldsymbol{a_x} - sin\phi_2 \boldsymbol{a_y}\right)d\phi_2$$

where r_1 and r_2 are position vectors on the two loops and $d\boldsymbol{s_1}$ and $d\boldsymbol{s_2}$ are small sections of the two loops. From (3.9) we can further derive some useful results for calculating the double integration in Neumann's Formula.

$$d\boldsymbol{s_1} \cdot d\boldsymbol{s_2} = Rrcos(\phi_1 - \phi_2)d\phi_1 d\phi_2$$

(3.10)

$$|R_{12}| = \sqrt{R^2 + r^2 + d^2 + H^2 - 2Rrcos(\phi_1 - \phi_2) - 2Rdcos\phi_1 + 2rdcos\phi_2}$$

With these two equations, we can calculate the mutual inductance between this two wire loops.

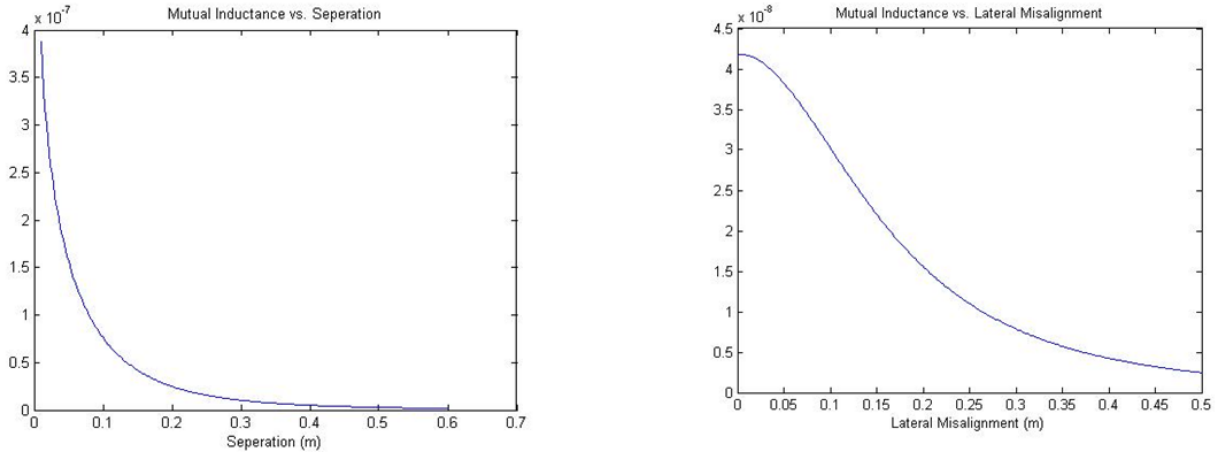

Figure 21: Relation between mutual inductance and lateral misalignment and separation

Figure 21 shows that the mutual inductance decreases quickly when the separation and lateral misalignment of the two wire loops increase, which is not surprising. From the figure, we would expect the mutual inductance to go to infinity when the distance between the two loops shrinks to zero, which is because the Neumann's Formula doesn't apply to two conductors that

are too close to each other, because when placed too close together, the charge and current distributions in one conductor will affect those in the other conductor, which nullifies the assumptions for Neumann's Formula.

3.1.3.2 Mutual inductance between two coils

Given the mutual inductance between two loops, we can evaluate the mutual inductance between two multiple-loop coils by summing the mutual inductance between each pair of loops

$$M_{ab} = \sum_{i=1}^{N_1} \sum_{j=1}^{N_2} M_{ij} \qquad (3.11)$$

where M_{ab} is the mutual inductance between two spirals and M_{ij}'s are the mutual inductance between the i^{th} loop in the first spiral and the j^{th} loop in the second spiral, which can be calculated using the formula derived in 3.1.3.1. Based on the geometrical model of our resonator, we can calculated the mutual inductance between two resonators as well as between resonator and driving and load loops. And most importantly, we can express the mutual inductance as a function of the distance between resonators such that, we can optimize the position of resonators in a wireless power transmission system.

3.1.4 Optimization

The optimization problem is formulated as

$$\max_{d} |G(\omega_0; d)| \tag{3.12}$$

where $G(\omega_0)$ is the transfer function from the source to load evaluated at the natural frequency of the resonators and d is the distance between the transmitter and the relay resonator. As this is a small optimization problem, we can use exhaustive search to find the maxima of the transfer function. In the simulation, the transmitter and receiver were separated by 20 cm and plots of maximum absolute value of transfer function vs distance between source and relay is presented with different load value.

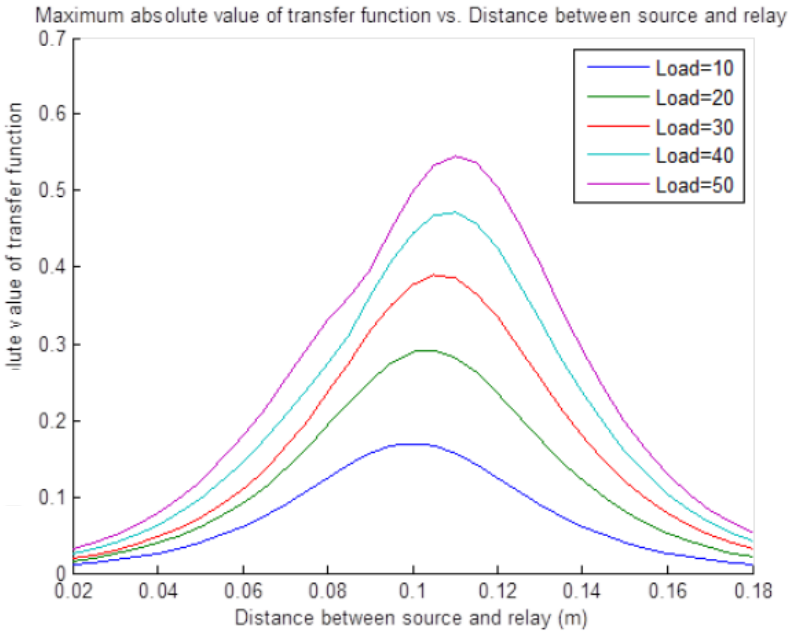

Figure 22 Calculation results of absolute value of transfer function at resonance vs. position of relay coil.

Based on this calculation, we can choose the optimal position for the relay coil such that the absolute value of transfer function can be maximized. And interestingly, this optimal position is dependent on the load value, and further study may be needed to identify their relationship in more detail.

3.2 EXPERIMENTS

To verify the result, I built a system shown in Figure 23, where the transmitter and receiver are fixed with a distance of 20 cm, while the relay can be moved freely on the rail and a network analyzer is used to measure the S_{21} and S_{11} parameters to compute the absolute value of transfer function at natural frequency

$$\left|G(\omega_0)\right| = \frac{S_{21}}{1 - S_{11}} \tag{3.13}$$

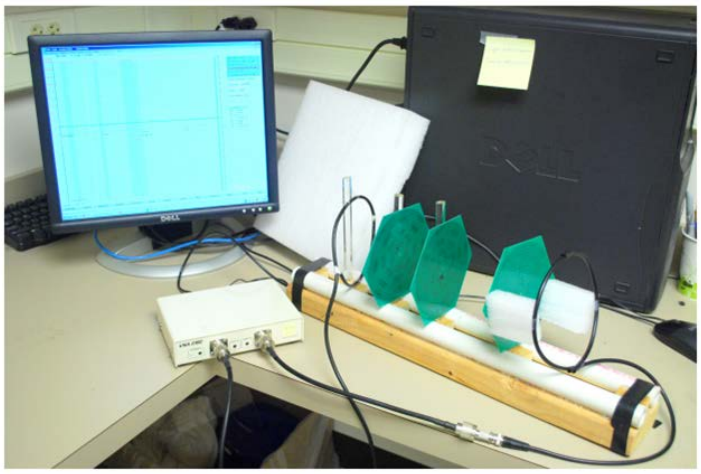

Figure 23: Experimental platform for 3-coil relayed system

The transmitter and receiver were separated with a distance of 20cm and the relay can be moved in between, four load values were tested in the experiment.

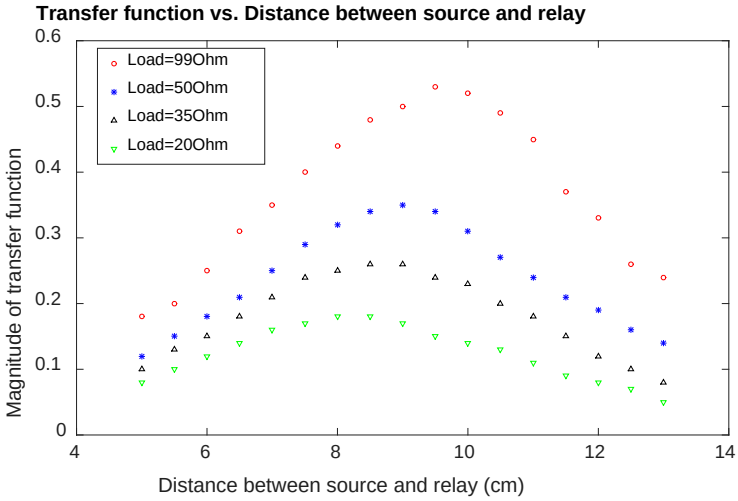

Figure 24. Calculation Results

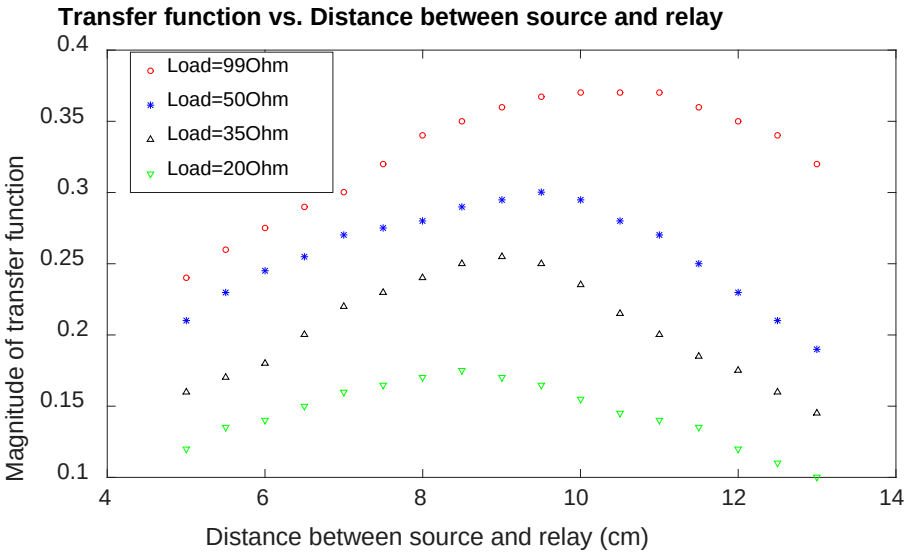

Figure 25. Experimental results

Comparing the experimental results to the calculation results, we can see that they predict similar locations for the relay coil except for the largest load case, where the experimental results shows larger distance to the transmitter than calculation. A closer investigation shows that all measured optimal position are a little bit to the right of the calculated result, also, the transfer function from measurement is also large then the calculation. Both case indicated that the

actually load is more likely to be larger than the value measured due to some other unaccounted sink of energy.

3.3 CONCLUSIONS

In this project, a transfer function based multiple resonator wireless power transmission system design method was introduced, when combined with mutual inductance analysis, this method is capable to find optimal location of the transmitters such that maximum transfer can be achieved. The method was then applied to obtain the optimal position of a relay coil in the three-resonator wireless power transmission system. The method shows accurate result compared with experimental verification and the result shows that even though the optimal relay positon is around the middle point between transmitter and receiver, it also varies with different load value.

4.0 FIELD-DRIVEN DESIGN OF A MULTIPLE-RESONATOR POWER TRANSMISSION PLATFORM

Position-free wireless power transfer system has been a hot research topic in the WPT area, as position-free is an essential characteristic that will largely increase the possible applications of the WPT technology. Despite the increased transmission distance compared to the inductive coupling method, a simple two-coil resonant coupling system still cannot be categorized as a position-free system, so a multiple transmitter system is needed. Due to the requirement of positon-free, the transmitter should be able to generate evenly distributed vertical component of the magnetic field in the interested area, such that the device can get charged at a constant speed no matter where it is in this range. Because of the importance of the evenness of magnetic field, a field driven design method was proposed, where the magnetic field generated by the transmitter can be approximated through Biot-Savart law so that the evenness of field can be maximized afterwards. This method was then utilized to optimize the design of a mat-based system for position-free wireless charging of biomedical implants. This system was originally designed for lab rodent experiments, so that the mice do not need to carry a battery and the implanted devices can receive sufficient and constant power wherever the mouse is. This chapter starts from a description of the original system, followed by the proposed method to optimize the design and experimental verification, and conclusions are provided in the end.

4.1 DESCRIPTION OF THE MULTI-RESONATOR POWER MAT

To increase the effective range of the wireless power transmission system, a straight forward idea is to increase the number of transmitters and following this idea, the power transmission mat was designed.

4.1.1 Transmission mat

For the same reason stated before, circular spiral coils were used in the design. And the transmission resonators are the same as the ones used in the 3-coil relayed system and will not introduced again here. The spiral is printed on a hexagonal PCB and can be used as a tile to form a large mat as shown in Figure 26. Here hexagon is not an arbitrary choice, rather it has been proved that this design will leave the smallest gap between resonators [37, 38].

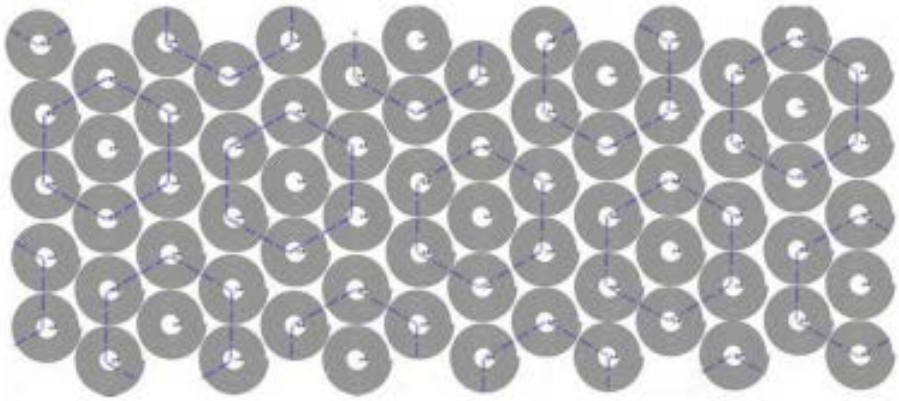

Figure 26. Sketch of the powering mat

In the experiment and analysis, it is not possible or necessary to directly work on an arbitrary large number of resonators. Rather, for a large mat, every one of the resonators can be treated as in the middle of the mat, except for those ones at the edge, and fortunately the edge

effect can either be ignored or can be solved by making the mat larger than the requested effective area. For this reason it is enough to examine only one single resonator. However, to make this resonator similar to one in the middle, a seven-resonator mat was implemented as shown in Figure 27 and forms the simplest unit for measurement and analysis. Also the measurement was only performed over the middle resonator for the previous reasoning.

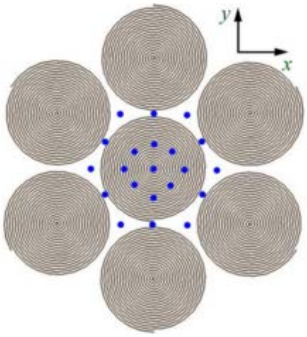

Figure 27. Sketch of a seven-resonator mat and the test points

4.1.2 Source loop design

To make the resonators reinforce each other, all the transmitters should have the same input. So a special source loop was designed to power the seven-resonator transmitter as in Figure 28.

Figure 28. The source loop

Seven loops were connected together with one loop beneath each resonator. The power was fed into the loops with two circular connectors. A gap was cut on each of the circular connectors so that they do not form a close loop on their own to prevent current flowing in these circles.

4.1.3 Receiving resonator design

The receiving resonator design has been a critical problem for implanted devices because the size of the receiver is limited. And to make the small receiver resonant at the same frequency as the relatively large transmitter is challenging. So the receiving resonator took a novel design as shown in Figure 29, rather than the traditional planar spiral coil. The receiving resonator consists three parts, which together form a cylinder box. The top and bottom are two circular spirals and the side surface is a solenoid, so this design makes full use of the volume to increase the inductance of the resonator so that the resonant frequency can be lowered. Another advantage of this design is that the resonator itself can be treated as the container of the electronic devices put inside, so more space is saved.

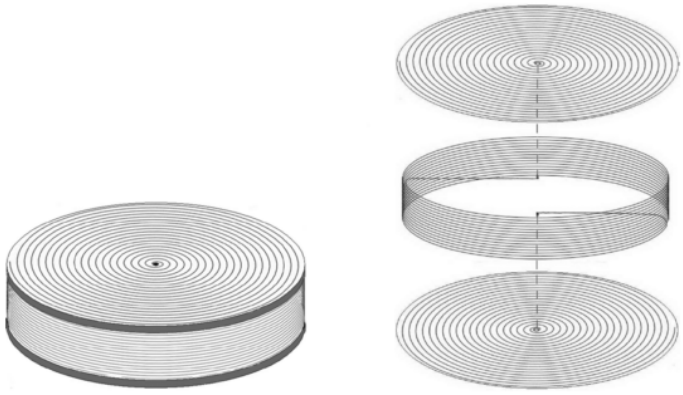

Figure 29. Sketch of the receiving resonator

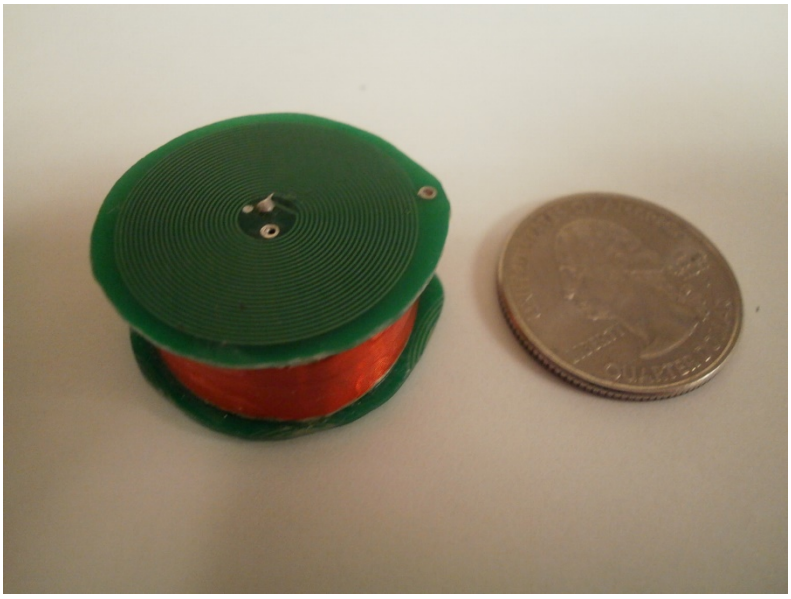

Figure 30. Receiving resonator

4.1.4 Preliminary test

Preliminary measurement was performed on this system with the test platform shown in Figure 31.

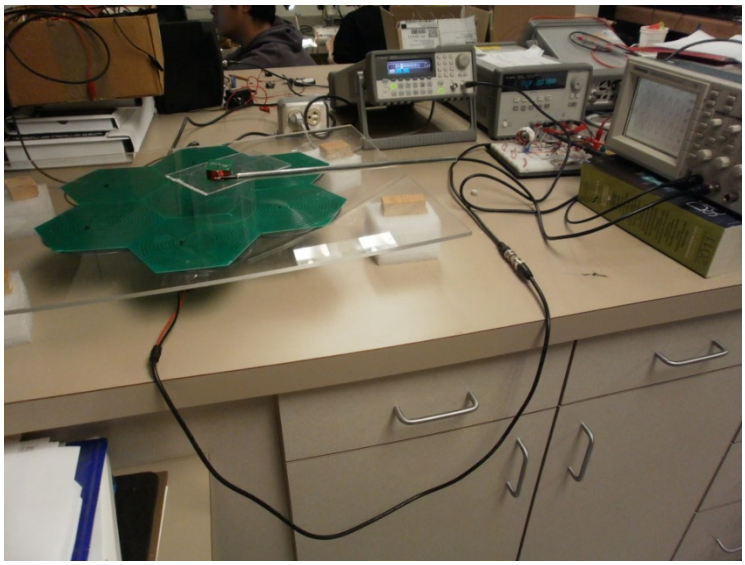

Figure 31. Test platform of the power mat system

The voltage at the receiver was performed with different distances between the transmitter and the receiver and the result is shown below.

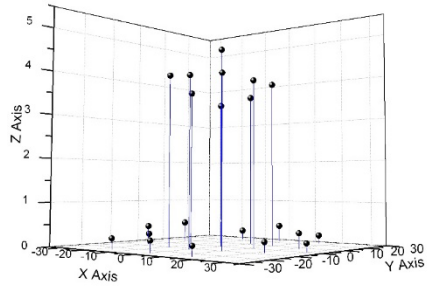

(a)

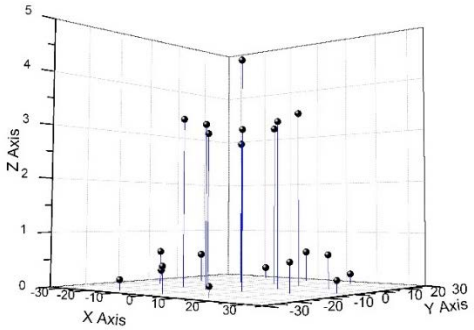

(b)

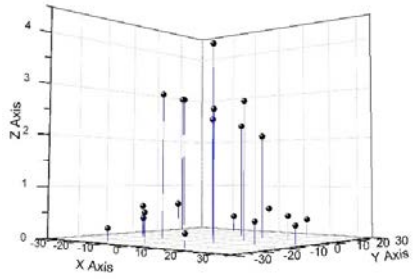

(c)

Figure 32. Measurement result with different distance between transmitter and receiver.

(a)3.2cm (b)4.2cm (c)5cm

The result shows that the voltage varies tremendously over the area of the center coil. Before we can talk about optimizing the platform, we need a method to evaluate the goodness of the platform theoretically. And in this dissertation, we directly evaluate the flatness of the magnetic field generated above the central transmitter, where the magnetic field can be approximated through Biot-Savart law. Detailed method to optimize the design is shown in the next section.

4.2 METHODS

4.2.1 Field evaluation

Magnetic field generated from a coil can be calculated from Biot-Savart law.

$$\mathbf{B}(\mathrm{r}) = \frac{\mu_0}{4\pi}\int_C Id\boldsymbol{l} \times \frac{\boldsymbol{r}'}{|\boldsymbol{r}'|^3} \tag{4.1}$$

And to make things easier, we utilize the concentric model discussed before to approximate the coil and the generated magnetic field is a superposition of the field of each loop. Figure 33 shows a sketch of how to calculate the magnetic field of a single loop.

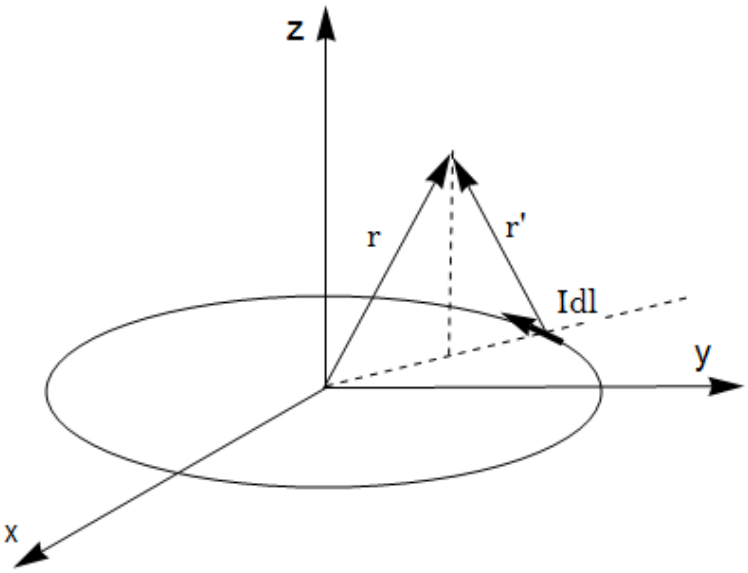

Figure 33. Sketch of magnetic field calculation for a single loop.

The magnetic field is evaluated at point r, with coordinates (ρ,ϕ,z) in the cylindrical coordinate system, (x, y, z) in the XYZ coordinate

And after calculation, we have [39]

$$\begin{aligned} \mathbf{B_x} &= \frac{\mathrm{Cxz}}{2\alpha^2\beta\rho^2}[(R^2+r^2)E(k^2)-\alpha^2K(k^2)] \\ \mathbf{B_y} &= \frac{Cyz}{2\alpha^2\beta\rho^2}[(R^2+r^2)E(k^2)-\alpha^2K(k^2)] \\ \mathbf{B_z} &= \frac{C}{2\alpha^2\beta}[(R^2-r^2)E(k^2)+\alpha^2K(k^2)] \end{aligned} \tag{4.2}$$

where $\alpha^2 = a^2+r^2-2arsin\theta$, $\beta^2 = a^2+r^2+2arsin\theta$, $\mathrm{k}^2 = 1-\alpha^2/\beta^2$, $\mathrm{C} = \mu_0 I/\pi$, and K(.) and E(.) are the complete elliptic integrals of the first and second kinds, respectively. For easier calculation, without loss of generality, the current is chosen such that $\mathrm{C} = 1$. With the single-loop magnetic field calculated, we can apply the superposition rule to get the field generated by a multi-loop circular coil. Since, for the application of recharging, the device is placed on the surface of the recharging tray, the receiver coil is always in parallel with the transmitter coil which is installed below the surface. As a result, the fluxes in the receiver coil are contributed by

the z component of the magnetic field. Therefore, we will focus on the z component of the magnetic field in the following analysis.

Applying this method, we can evaluate the magnetic field of the seven-transmitter powering platform, Figure 34 shows a visualized magnetic field with different distances between transmitter and the surface where field was evaluated.

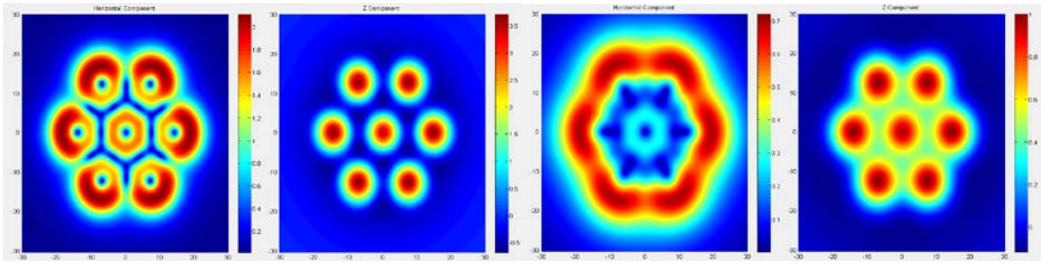

(a) (b)

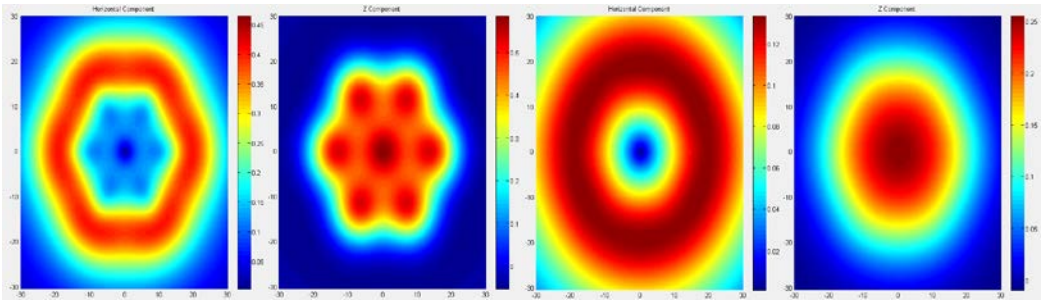

(c) (d)

Figure 34. Magnetic distribution with different heights between evaluating plane and transmitter. (a)3.25cm (b)7.25 (c)10.25 (d)20.05cm. With horizontal components in the left image and vertical components in the right.

Measurement shows that the height between the evaluating plane and the transmitter controls that variation of the magnetic field as well as the distribution between horizontal component and z component. As the z component contributes more to the coupling between the transmitter and receiver, we examine the z component more closely. When height is increasing,

the flatness of the magnetic field also improves at first. However, when the height is too large, the magnetic field distribution becomes similar to that of a larger spiral, which hurts both the flatness and magnitude of the magnetic field. When the height is too small, although the peak magnitude is larger, the z component is actually inversed at the gap between resonators, which means large fluctuation of the magnetic field. Another design parameter is the distance between resonators, and in the next section we will optimize the evenness of the vertical magnetic field with respect to the high of the evaluation plane above the transmitter h and the distance between resonators d.

4.2.2 Optimization

The optimization problem can be formulated as

$$\min_{h,d} std(B_z)/abs(mean(B_z)) \quad \text{s.t. } h > 0,\ d > 2*R \tag{4.3}$$

where R is the outer radius of the resonators. The objective function is chosen such that the tradeoff between evenness and amplitude of the magnetic field can be considered. And because of the symmetry, the field only needs to be calculated along a radius from the center at different height.

As the objective function can only be evaluated rather than having a closed form expression, also the objective function is so complicated that multiple local minimum is expected, the formulated optimization problem cannot be solved using simple gradient based algorithms. But there are metaheuristic algorithms to handle this kind of problem, and in this dissertation, we used stimulated annealing method in the global optimization toolbox of Matlab.

In the optimization, the lower bound of distance between adjacent resonator d is set to be twice the radius of the coil, or 14cm, and the upper bound is 28cm, while the lower bound and upper bound of the distance between probe and the power mat h are 1cm and 10cm respectively and the initial value of d and h are set to be 21cm and 5cm respectively. After optimization, we got

$$d_{opt} = 14cm$$
$$h_{opt} = 10cm$$
$$f_{opt} = 0.0455$$

So, the system is optimized when d is at its minimal value while h is maximal. And the optimized vertical component of the magnetic field can be calculated directly with d and h known.

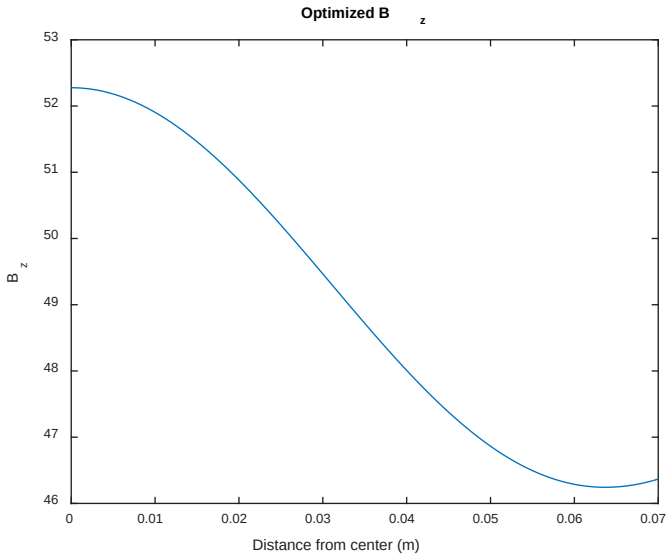

Figure 35. Optimized B_z

The Bz shows a relative change of less than 15% which evener than the previous design. The minimal value does not happen at 7cm as expected and it's because this is only a seven-coil platform. With larger number of resonators, we would expect the magnetic field to be symmetric.

4.3 EXPERIMENTS

For experimental verification, the original platform was utilized, by measuring the induced voltage in the small receiving coil, we are able to estimate the vertical magnetic field,

$$V = -\frac{\partial \phi}{\partial t} = -N\frac{\partial \overline{B}_z S}{dt} \propto B_z \tag{4.4}$$

From equation (4.4) we can see that when the measuring coil is sufficiently small, and the system is driven by sinusoidal input, then the induced voltage in the measuring coil is proportional to the local B_z and as our objective function cancels out the constant relating these two values, we can directly evaluate the cost function with V instead of B_z as the argument and compare with the calculation result.

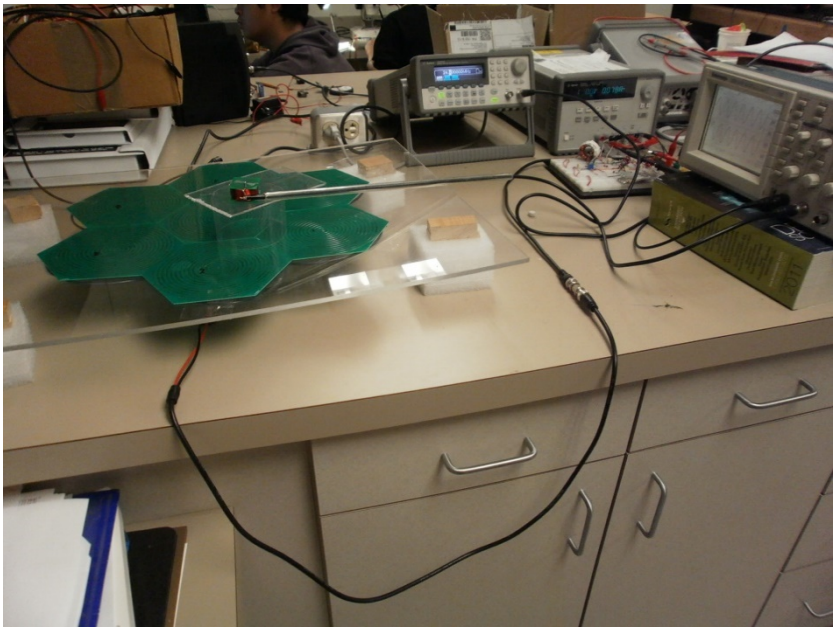

Figure 36 Experimental platform for measuring magnetic field distribution.

To compare the measured voltage with the calculated Bz, we need to normalized both of them on to the same scale, as they are supposed to be proportional to each other.

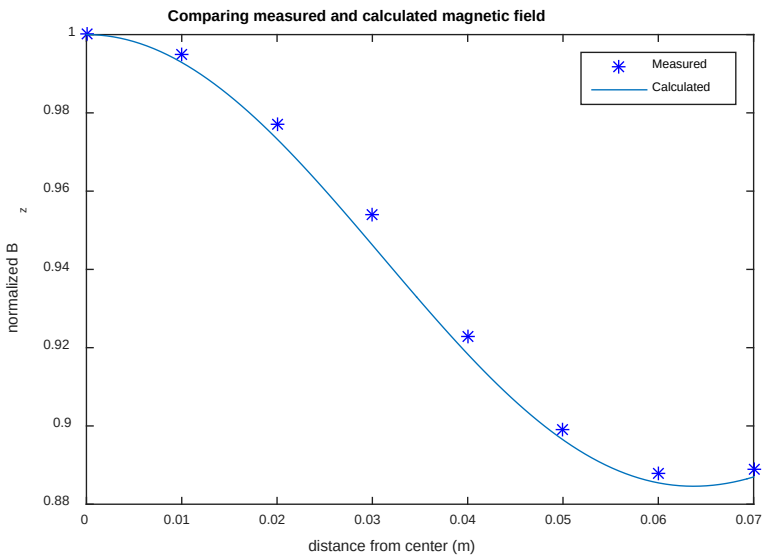

Figure 37. Comparing measured and calculated vertical magnetic field

Figure 37 shows that the measured data matches the calculated ones very well, except for that the measured data tends to be larger than the calculated ones, which is because the receiver, due to its 3D structure can capture a small portion of horizontal field as well, such that when we normalize it to the center value where the horizontal component is almost zero, the other positions will have larger than expected field.

4.4 CONCLUSIONS

In this part, a magnetic field-driven multiple-resonator design was presented, where the magnetic field generated by multiple-transmitter platform can be evaluated through Biot-Savart formula. Then the magnetic field can be optimized with respect to some geometric parameters of the system so that the required properties can be achieved. This method is suitable for designing position-free charging platform, where the magnetic field should be even enough such that

constant charging speed can be achieved. In the experimental part, a seven-coil transmitter platform was optimized for better evenness of vertical magnetic field. Even though multiple-coil transmitter is often used for position-free wireless charging, the vertical magnetic component of such platform is not quite uniform, even after optimization. Future research direction may involve non-uniform coil as possible approach for position-free charging, which already showed promising results in recent works [42, 43].

5.0 UNIFIED CHANNEL FOR DATA AND POWER TRANSMISSION

In this last project, a unified data and power transmission channel will be implemented, where the power receiver side utilize ASDM and load modulation to transmit data back to the reader. The advantage of this method is that the transmitted data is analog thus no clock is needed, and the load modulator has a much simpler form compared to other modulation devices.

5.1 SYSTEM MODELING

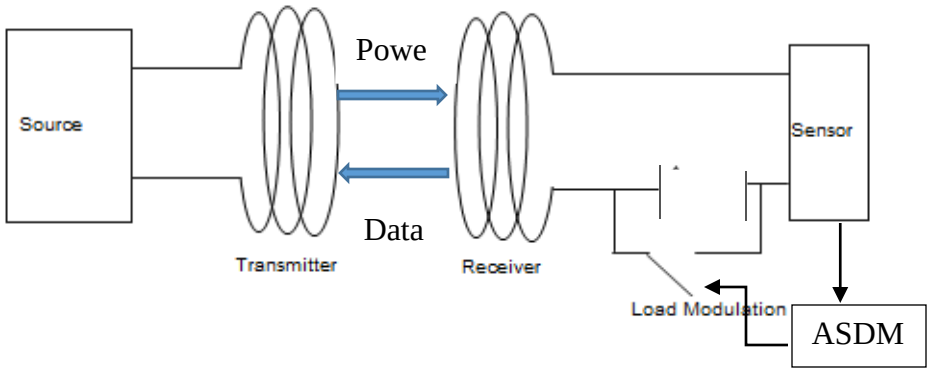

Figure 38. Structure of unified data and power transmission system

In this structure, the power path is the same as before, and the data path is to transform the measured data to a voltage signal with only two voltage levels through ASDM, and then use this pulse train to control the load on the receiver side, such that the data can be sensed from

outside. As the ASDM is a separated part, let's investigate more on the load modulation, which is highly integrated into wireless power transfer path.

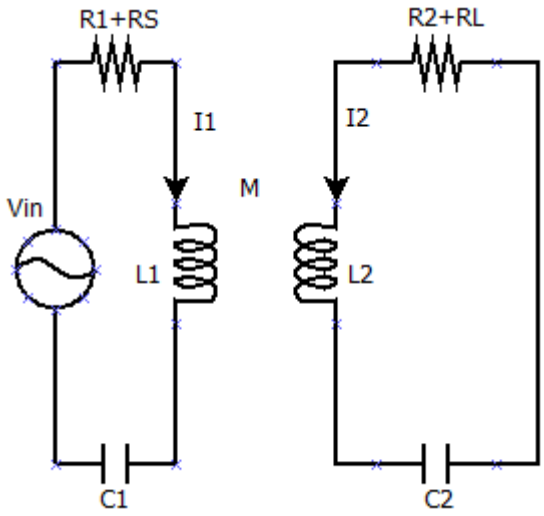

Figure 39. Equivalent circuit of a typical two-coil wireless power transmission system.

The above figure shows the equivalent circuit of a typical two coil wireless power transmission system, the parameters are defined as before, and the only difference is that the capacitance C_2 is adjustable and can switch between two values when controlled by a pulse wave. From KVL we get the following equations:

$$\begin{cases} vs = i_1(R_1 + R_S) + L_1\dfrac{di_1}{dt} + M\dfrac{di_2}{dt} + \dfrac{Q_1}{C1} \\ 0 = i_1(R_2 + R_L) + L_2\dfrac{di_2}{dt} + M\dfrac{di_1}{dt} + \dfrac{Q_2}{C_2} \\ i_1 = \dfrac{dQ_1}{dt} \\ i_2 = \dfrac{dQ_2}{dt} \end{cases}$$

One thing to be noted is that rather than using voltage across capacitors as state variables as in normal KVL equations, charge stored in capacitors are used instead. The reason is that with C2 switching between two values, the voltage across C2 is subject to instantaneous jump such that it is not differentiable while the change of charge is still smooth.

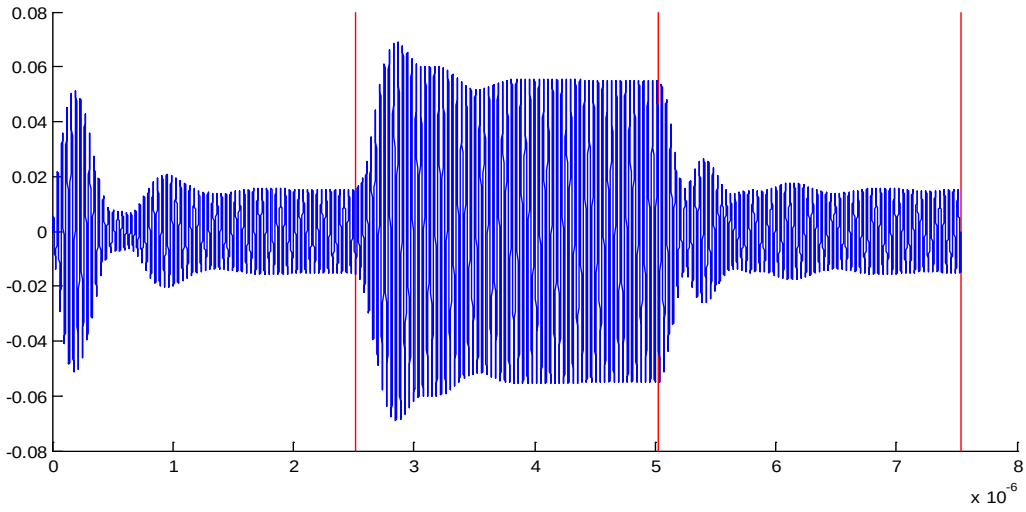

Figure 40. Simulation of load modulation on the equivalent circuit.

Figure 40 shows the simulation output of I1, where the red lines show the switch time of C2. As can be seen, a small change of C2 can cause a substantial change in I1. However, due to the asymmetry of the circuit, i. e. C2 is of different values on the rising and falling edge, the detected pulse width may be inaccurate, which is fatal for recovery of ASDM modulated data, as the information is totally stored in the switching time.

5.2 MODEL REFERENCED EDGE DETECTION

To solve the above problem and also in hope of increasing the data rate, a model referenced edge detection algorithm was developed.

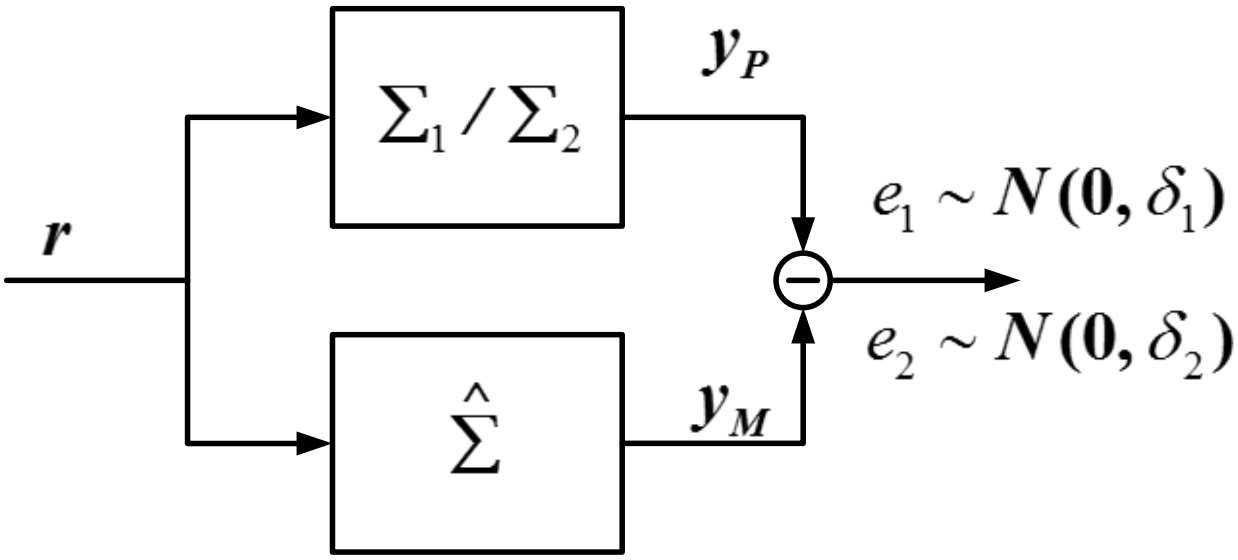

Figure 41. Model referenced edge detection system.

Here the Σ_1 and Σ_2 are mathematical models corresponds to the two status of the real WPT system, caused by changing of load C_2. So that the mathematical model switches between Σ_1 and Σ_2 whenever a change of load is detect, which means the mathematical model is always tracking the status of the plant. Such that instead of waiting for the edge to settle down, we can detect the next edge even in the transient time, as long as the mathematical model detected the previous edge already and the error between these two outputs started to shrink.

Model referenced edge detection mechanism is also capable of solving the problem of different delay of edge detection on the rising and fallowing edges. Problem is shown in Figure 42, where the blue and green curve shows the output from the real plant and the mathematical

model respective, the red vertical lines show the times when load changes value, and black circles is the times when the change of load is detected by observing the error between the two outputs.

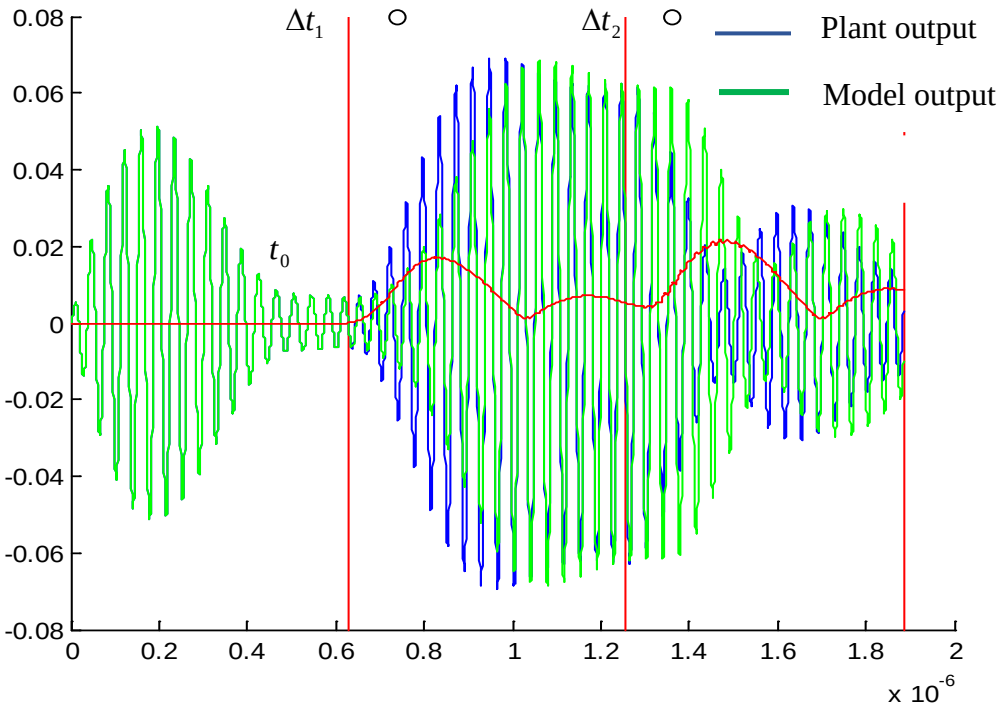

Figure 42. Edge detection

Let's denote the output of the plant as p(t), and the output from the model m(t). Apparently, p(t) senses the change of load earlier than m(t) by Δt_1 on the rising edge and Δt_2 on the falling. Without loss of generality, we only consider rising edge in the following analysis. Because of delay, we have the amplitude of $p(t_0) \approx m(t_0 + \Delta t_1)$, thus for off-line edge detection, we can halt $m(t)$ at time $t_0 + \Delta t_1$ and let $m(t)$ catch up with $p(t)$ and the elapsed time in this process should be close to Δt_1. Thus we can trace back from the time of edge

detection to the time of edge occurrence. Not only the time of edge occurrence can be detected, we also reduced the error between this two outputs to almost zero at $t_0 + \Delta t_1$ so that the system is ready to detect the next edge, instead of waiting for the error to diminish.

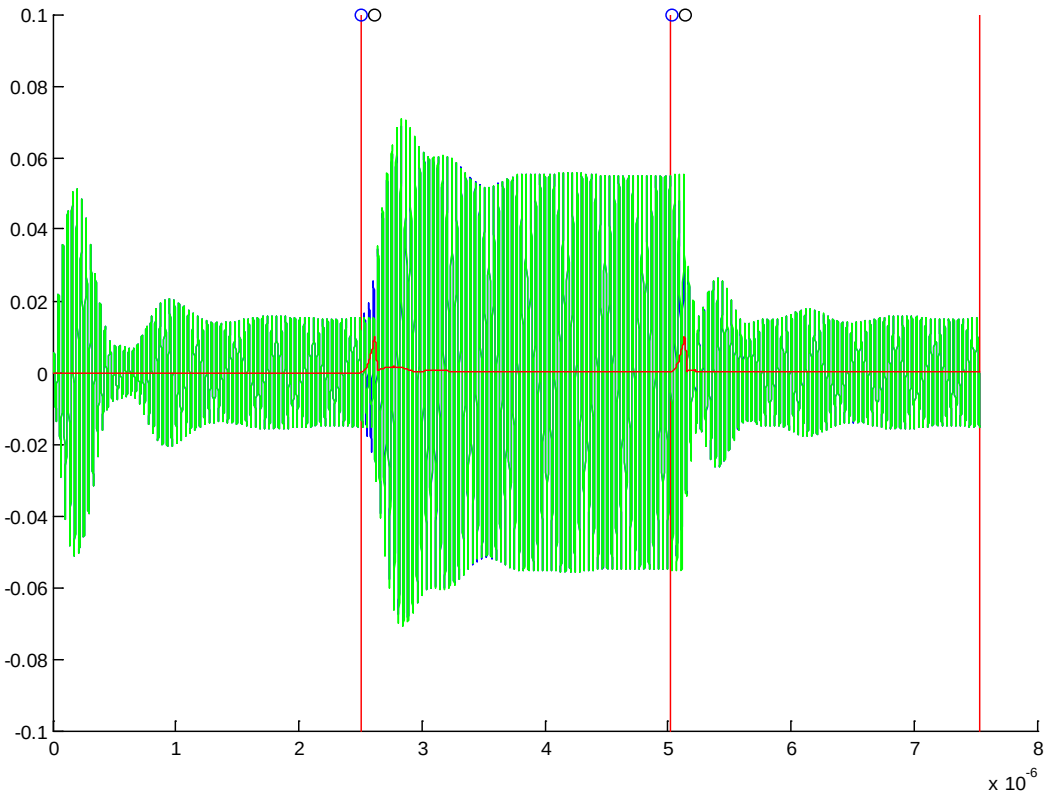

Figure 43. Result from modified edge detection algorithm

As can be seen the modified algorithm can detect edge at blue circles, which are more accurate than the black ones as in the simply error thresholding algorithm. Also the red error curve decrease to almost 0 at the time of $t_0 + \Delta t_1$ as we expected, which could increase the possible data rate. The drawback of this approach is that it cannot be done in real time, however, this shouldn't be a problem for applications where batch processing is also acceptable.

5.3 EXPERIMENTS

In the experiment, a premeasured ECG signal was transmitted through the power channel to the receiver side.

5.3.1 ASDM

ASDM algorithm was first test on the ECG signal, which was obtained from MIT-BIH Arrhythmia Database [40, 41]. The sampling rate is 360 Hz, which is not enough for ASDM modulation, so the signal was interpolated so a sampling rate of 18000 Hz, and the parameter of the ASDM modulator was chosen such that the cutoff frequency is 30 Hz. The modulation result is shown in Figure 45, and the signal was then normalized to between 0 and 5 V to control an analog switch for load modulation.

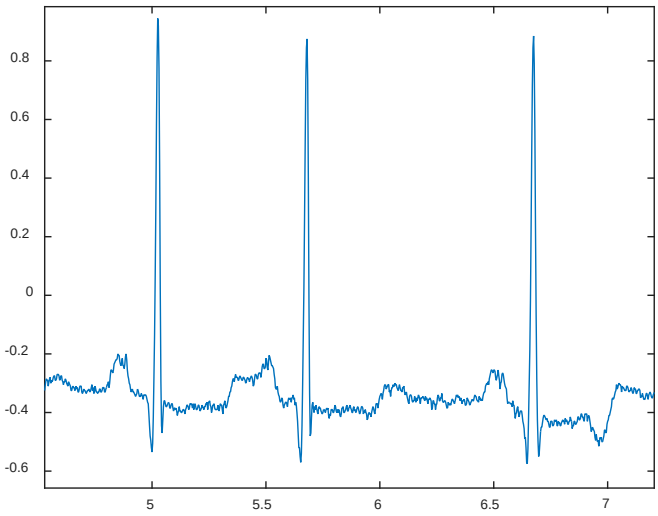

Figure 44. Original ECG signal

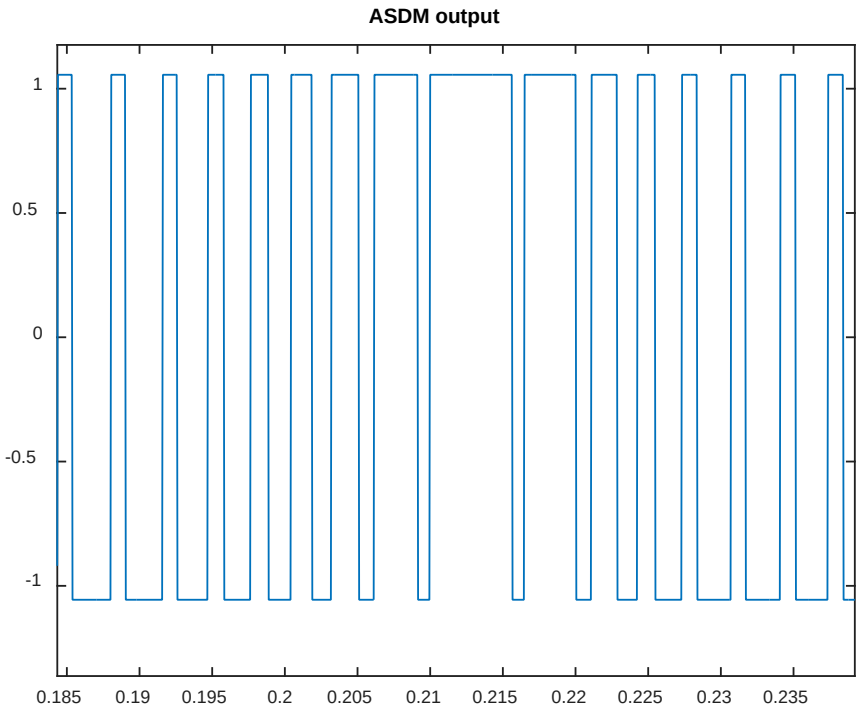

Figure 45. ASDM modulated ECG signal

5.3.2 Output the modulated signal

The control signal was outputted through an NI daq device shown in Figure 46.

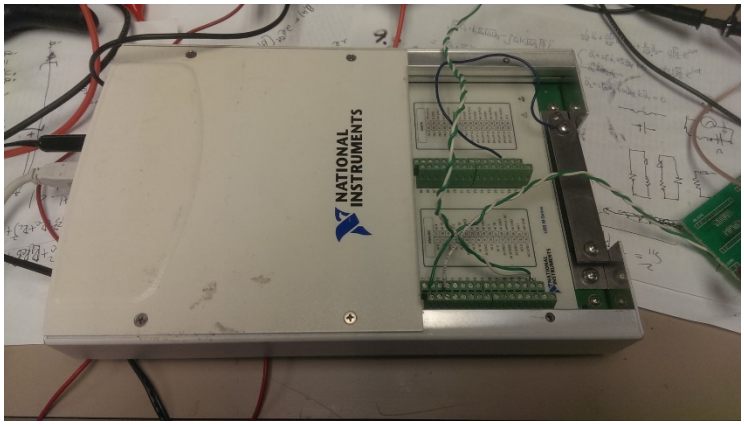

Figure 46 Data acquisition device from National Instruments

Matlab provided a DAQ toolbox which has interfaces to control the NI devices, such that the modulated signal in Matlab can be directly outputted from the device, and the measured modulation output is shown in Figure 47

Figure 47. Modulation output from NI daq device.

5.3.3 Experiment platform

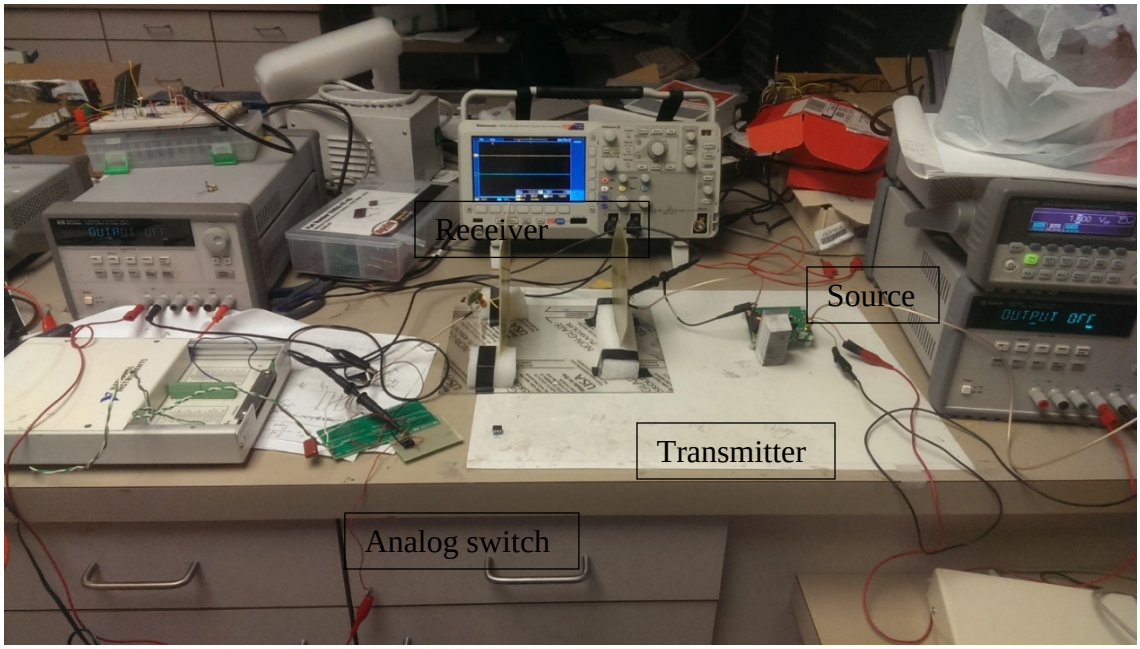

Figure 48. Experiment platform

The experiment platform was shown in Figure 48, where the pulse train outputted from the daq device was utilized to control an analog switch, which modifies the load on the receiver and the voltage on transmitter was recorded for latter processing.

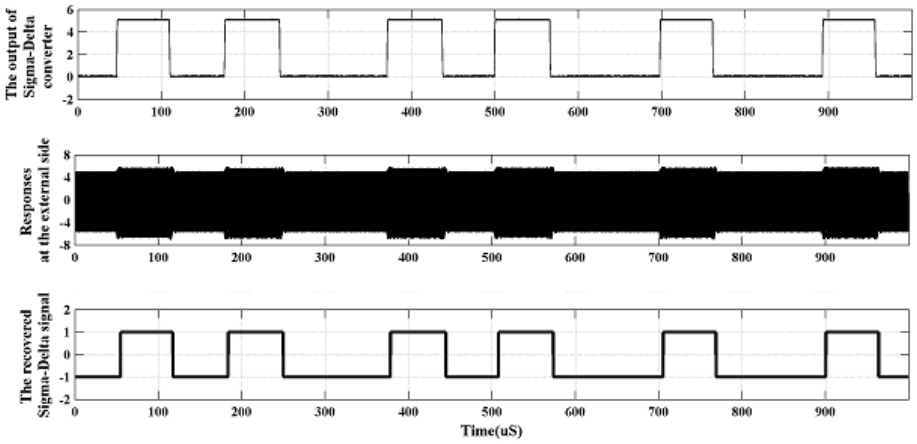

Figure 49. Experimental Result.

Based on the recovered pulse train, the original ECG data can be recovered through the ASDM demodulator introduced in chapter 2. The recovered signal shows less high frequency component due to the low cutoff frequency in the ASDM procedure. Other than that the recovered signal matches the original system very well.

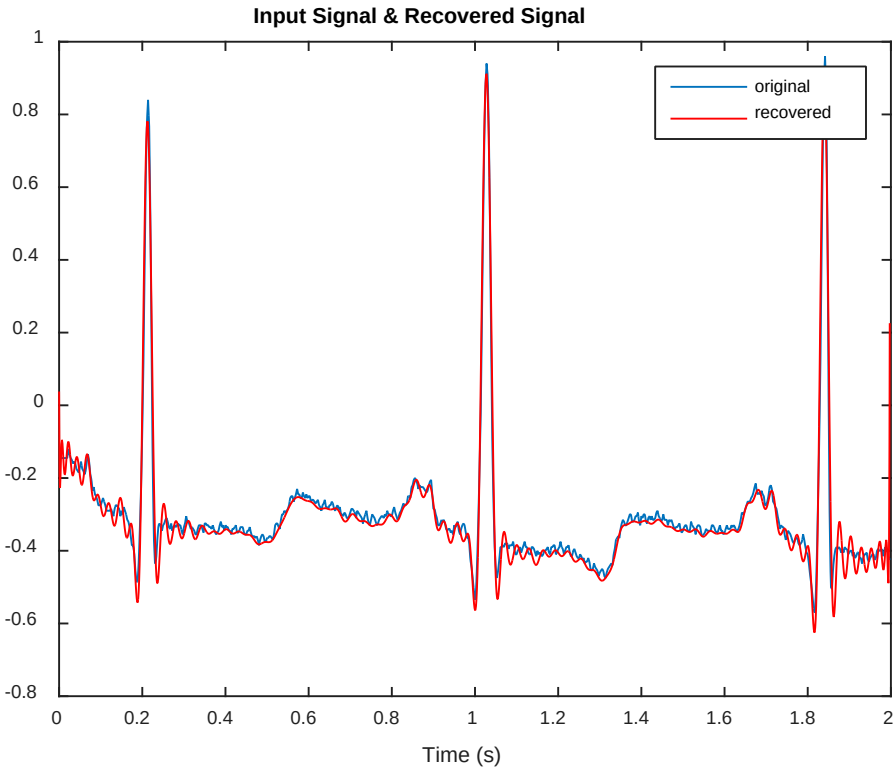

Figure 50. Input and recovered signal

5.4 CONCLUSIONS

In this part, a unified data and power transmission channel was presented, where ASDM and load modulation were utilized to transmit data back from the power receiver through the wireless

power channel. A novel model referenced edge detection algorithm was also implemented to detect the actual time of load change, despite the narrow bandwidth of the power channel ruins the sharpness of every edge of the signal. The algorithm is also capable to increase the possible data rate by enabling the system to change state before the signal is settled. It shows good results when the mathematical model matches the plant well, which leads to future research direction of real-time system identification of the wireless power transmission system.

6.0 CONTRIBUTIONS AND SUGGESTED FUTURE RESEARCH

In this thesis, three projects were fulfilled, where the first two focuses on multiple-resonator WPT system design and the third is to unify the wireless power and data transmission channel. The achievement is as follows:

Firstly, a transfer function based multiple-resonator WPT system design method was proposed and utilized to find the optimal position of the relay coil in a three-resonator WPT system. This method provides a convenient tool for optimizing a WPT system geometrically for better transfer rate.

In the second project, a magnetic field-driven design method was introduced for optimizing position-free WPT systems, where the magnetic field generated by the transmitter should be evenly distributed over the charger such that the receiver can get charged with constant speed. This method is especially useful for systems with spiral coils, as their magnetic field can be evaluated easily. The method was applied to optimize the design of a seven-coil power transmitter, however, the result shows that the multiple-coil platform is not capable of generating uniform magnetic field due to the interacting between adjacent coils.

Lastly, a unified data and power transmission channel was presented, where data were transmitted using asynchronous sigma-delta modulation and load modulation through the magnetic resonant wireless power transmission system. Result shows that it can transmit ECG data very well. And a novel model referenced edge detection algorithm was implemented to

identify the switch time of the load modulator. The drawback of this method is that it rely on the accuracy of the referenced model.

Based on the problems in the current state, two future research directions would be suggested. Firstly, to utilize a single large coil for position-free platforms. Many researches have been done about non-uniform resonators, maybe non-planar coils should also be considered. The second direction is to do real time system identification of a wireless power transmission system, which is useful for both data transmission and impedance matching etc.

BIBLIOGRAPHY

[1] N. Tesla and D. H. Childress, “The fantastic inventions of Nikola Tesla (Lost Science),” Adventures Unlimited Press, June 30, 1993

[2] N. Tesla, “Apparatus for transmitting electrical energy,” U.S. Patent 1119732, 12, 1914.

[3] P. E. Glaser, “Power from the sun: It’s future,” Science, vol. 162, pp. 867-886, 1968

[4] “Space solar power,” http://www.brightgreencities.com/v1/en/bright-green-book/estados-unidos/energia-solar-espacial/.

[5] “Wireless electricity products spark a new industry,” http://www.powerbeaminc.com/2010-05-07.php.

[6] G. Franceschette, A. Massa, and P. Rocca, “Innovative antenna systems for efficient microwave power collection," in IMWS-IWPT2011 Proceedings, 2011, pp. 13-14.

[7] J. M. Fernandez and J. A. Borras, “Contactless battery charger with wireless control link," U.S. Patent 6,184,651, 02, 2001.

[8] L. Ka-Lai, J. W. Hay, and P. G. W. Beart, “Contactless power transfer," U.S. Patent7, 042,196, 05, 2006.

[9] A. Karalis, J. D. Joannopoulos, and M. Solja_ci_c, “Efficient wireless non-radiative mid-range energy transfer," Annals of Physics, vol. 323, pp. 34-48, 2008.

[10] A. Kurs, A. Karalis, R. Moffatt, and et al, “Wireless power transfer via strongly coupled magnetic resonances," Science, vol. 317, pp. 83-86, 2007.

[11] L. C. Benjamin, F. H. James, and C. G. Seth, “Magnetic resonant coupling as a potential means for wireless power transfer to multiple small receivers," IEEE Transactions on Power Electronics, vol. 24, pp. 1819-1825, 2009.

[12] A. Kurs, R. Moffatt, and M. Soljacic, “Simultaneous mid-range power transfer to multiple devices," Applied Physics Letters, vol. 96, pp. 044 102-044 103, 01 2010.

[13] J. Kim, H. Son, D. Kim, K. Kim, and Y. Park, “Analysis of wireless energy transfer to multiple devices using cmt," in Microwave Conference Proceedings (AMPC), 2010 Asia-Pacifc, 2010, pp. 2149-2152.

[14] A. P. Sample, D. A. Meyer, and S. J. R., “Analysis, experimental results and range adaptation of magnetically coupled resonators for wireless power transfer," IEEE Transactions on Industrial Electronics, vol. 58, pp. 544-554, 02 2011.

[15] H. Kim, S. Kang, S. Cheon, M. Lee, and T. Zyung, “Wireless power transmission to multi devices through resonant coupling," in International Conference on Electrical Machines and Systems (ICEMS), 2010, pp. 2000-2002.

[16] T. C. Beh, T. Imura, M. Kato, and Y. Hori, “Basic study of impoving efficiency of wireless power transfer via magnetic resonance coupling based on impedance matching,” in IEEE International Symposium on Industrial Electronics, 2010, pp. 2011-2016.

[17] F. Zhang, S. A. Hackworth, W. Fu, and M. Sun, “The relay effect on wireless power transfer using witricity," in 14th Biennial IEEE Conference on Electromagnetic Field Computation (CEFC), 05 2010, p. 1.

[18] M. Dionigi and M. Mongiardo, “E_ciency investigations for wireless resonant energy links realized with resonant inductive coils," in German Microwave Conference, 2011, pp. 1-4.

[19] H. Hirayama, Y. Okuyama, and K. Kikuma, N. Sakakibara, “A consideration of equivalent circuit of magnetic-resonant wireless power transfer," in Proceedings of the 5th European Conference on Antennas and Propagation (EUCAP), 2011, pp. 900-903.

[20] S. Shimokawa, H. Kawano, K. Matsui, A. Uchida, and M. Taguchi, “A numerical study of power loss factors in resonant magnetic coupling," in IMWS-IWPT2011 Proceedings, 2011, pp. 219-222.

[21] Y. Son, J. Kim, Y. Park, and K. Kim, “E_ciency analysis and optimal design of a circular loop resonant coil for wireless power transfer," in Asis-Paci_c Microwave Conference Proceedings (APMC), 2010, pp. 849-852.

[22] T. Imura and Y. Hori, “Maximizing air gap and e_ciency of magnetic resonant coupling for wireless power transfer using equivalent circuit and neumann formula," IEEE Transactions on Industrial Electronics, vol. 58, pp. 4746-4752, 2011.

[23] K. E. Koh, T. C. beh, T. Imura, and Y. Hori, “Multi-receiver and repeater wireless power transfer via magnetic resonance coupling-impedance matching and power division utilizing impedance inverter," in 15th International Conference on Electrical Machines and Systems (ICEMS), 10 2012, pp. 1-6.

[24] H. Lim, K. Ishida, M. Takamiya, and T. Sakurai, “Positioning-free magnetically resonant wireless power transmission board with staggered repeater coil array (srca)," in IMWS-IWPT2012 Proceedings, 2012.

[25] K. Murari, C. M. Sauer, M. Stanacevic, G. Cauwenberghs, and N. Thakor, "Wireless multichannel Integrated Potentiostat for Distributed Neurotransmitter Sensing," Proceedings of IEEE Engineering in Medicine and Biology 27th Annual Conference, Shanghai, China, Sep. 1-4, 2005.

[26] C. Sauer, M. Stanacevic, G. Gauwenberghs, and N. Thakor, "Power harvesting and telemetry in CMOS for implanted devices," IEEE Transactions on Circuit and Systems, vol 52, No. 12, Dec. 2005, pp 2605-2613.

[27] M. Mollazadeh, K. Murari, G. Cauwenberghs, and N. Thakor, "Wireless micropower instrumentation for multimodal acquisition of electrical and chemical neural activity," IEEE Transactions on Biomedical Circuits and Systems, vol. 3, No. 6, Dec. 2009, pp 388-397.

[28] E. Tolstosheeva, J. Hoeffmann, J. Pistor, D. Rotermund, et al, "Towards a wireless and fully-implantable ECog system," IEEE Transducers 2013, Barcelona, Spain, 16-20 June 2013, pp 384-387

[29] R. Carta, and R. Puers, "Wireless power and data transmission for robotic capsule endoscopes", 18th IEEE Symposium on Communications and Vehicular Technology in the Benelux (SCVT), Nov. 2011, pp 1-6.

[30] S. Noguchi, M. Inamori, and Y. Sanada, "Data transmission for resonant-type wireless power transfer," 14th International Symposium on Wireless Personal Multimedia Communications (WPMC), Oct 2011, pp 1-5.

[31] H. A. Haus, and W. Huang, "Coupled-mode theory," in Proceedings of IEEE, vol. 79, 1991, pp. 1505-1518,

[32] H. A. Haus, "Waves and fields in optoelectronics," Prentice-Hall: New Jersey, 1984.

[33] S. Senay, "Signal reconstruction from nonuniform samples using prolate spheroidal wave functions: theory and application," PhD dissertation, Swanson School of Engineering, University of Pittsburgh, 2011

[34] S. Su, "Asynchronous signal processing for compressive data transmission,", Master thesis, Swanson School of Engineering, University of Pittsburgh, 2011

[35] A. A. Lazar, "Recovery and sensitivity analysis of time encoded bandlimited signals," IEEE Transactions on Circuits and Systems-I, vol. 51, No. 10, Oct. 2004.

[36] R. Want, and S. Clara, "An introduction to RFID technology," Pervasive Computing, IEEE, vol. 5, issue 1, Feb. 2006, pp 25-33

[37] Q. Xu, Z. Gao, H. Wang, J. He, Z. Mao and M. Sun, "Batteries not included: a mat-based wireless power transfer system for implantable medical devices as a moving target," Microwave Magazine, IEEE, vol. 14, issue 2, Mar. 2013, pp. 63-72.

[38] Q. Xu, H. Wang, Z. Gao, Z. Mao, J. He, and M. Sun, “A Novel Mat-based system for position-varying wireless power transfer

[39] J. Simpson, J. Immer, and R. Youngquist, “Simple analytic expression for the magnetic field of a circular current loop”, NASA Technical Document Collection 2011, document ID: 20010038494.

[40] G. B. Moody, and R. G. Mark. “The impact of the MIT-BIH Arrythmia Database,” IEEE Eng in Med and Biol 20(3): 45-50 (May-June 2001)

[41] Goldberger AL, Amaral LAN, Glass L, Hausdorff JM, Ivanov PCh, Mark RG, Mietus JE, Moody GB, Peng C-K, Stanley HE. PhysioBank, PhysioToolkit, and PhysioNet: Components of a New Research Resource for Complex Physiologic Signals. Circulation 101(23):e215-e220 [Circulation Electronic Pages; http://circ.ahajournals.org/cgi/content/full/101/23/e215]; 2000 (June 13).

[42] J. Casanova, Z. Low and J. Lin, “Transmitting coil achieving uniform magnetic field distribution for planar wireless power transfer system,” in Radio and Wireess Symposium, Dan Diego, CA, 2009, pp. 530-533

[43] E. Waffenschmidt, “Free positioning for inductive wireless power system,” in Energy Conversion Congress and Exposition (ECCE), 2011 IEEE, 2011, pp. 3480-3487.